

University of Central Florida

**STARS**

---

Graduate Thesis and Dissertation 2023-2024

---

2024

## **Spatial Variability of Hydrodynamics within *Crassostrea virginica* (Eastern oyster) Reefs: Investigating the Effect of Canopy Density on Flow and Turbulence.**

Manisha Thenuwara  
*University of Central Florida*

Find similar works at: <https://stars.library.ucf.edu/etd2023>  
University of Central Florida Libraries <http://library.ucf.edu>

This Masters Thesis (Open Access) is brought to you for free and open access by STARS. It has been accepted for inclusion in Graduate Thesis and Dissertation 2023-2024 by an authorized administrator of STARS. For more information, please contact [STARS@ucf.edu](mailto:STARS@ucf.edu).

---

### **STARS Citation**

Thenuwara, Manisha, "Spatial Variability of Hydrodynamics within *Crassostrea virginica* (Eastern oyster) Reefs: Investigating the Effect of Canopy Density on Flow and Turbulence." (2024). *Graduate Thesis and Dissertation 2023-2024*. 460.  
<https://stars.library.ucf.edu/etd2023/460>

SPATIAL VARIABILITY OF HYDRODYNAMICS WITHIN CRASSOSTREA VIRGINICA (EASTERN OYSTER) REEFS:  
INVESTIGATING THE EFFECT OF CANOPY DENSITY ON FLOW AND TURBULENCE

by

MANISHA NIRMAL THENUWARA  
B.S. University of Ruhuna, 2020

A thesis submitted in partial fulfillment of the requirements  
for the degree of Master of Science  
in the Department of Civil, Environmental and Construction Engineering  
in the College of Engineering and Computer Science  
at the University of Central Florida  
Orlando, Florida

Spring Term  
2024

Major Professor: Kelly Kibler

© 2024 Manisha Thenuwara

## ABSTRACT

Oysters are ecosystem engineers that shape coastal aquatic environments through hydrodynamic influence, which is governed by the reef structure. Hydrodynamic studies have investigated effects of oyster reefs as whole systems, overlooking the spatial variability inherent in canopy structures. In this research, a field investigation was undertaken to characterize spatial variability of flow dynamics within a single eastern oyster (*Crassostrea virginica*) reef and query how the local canopy density influences the hydrodynamic environment. High-resolution flow measurements were taken within and above the oyster canopy over a range of flow conditions. Hydrodynamics were compared across reef locations as the oyster canopy density increased from sparse to very dense. Unique hydrodynamic behaviors were observed within and above all canopies. For example, flow attenuation was more complete within the canopy (70%-99% attenuation of incident flows) as compared to above (48%-65%). Canopies consisting of moderately dense to dense clusters of oysters exhibited similar hydrodynamic behaviors, characterized by high levels of flow attenuation (64%-97%) and turbulent mixing (mean turbulence intensity up to 30 times the shear velocity). Locations with sparse canopy density and the greatest density, where oysters were packed homogeneously rather than clustered, also greatly attenuated flows (70%-99% attenuation of incident flows) but were characterized by lower turbulent mixing (mean turbulence intensity 1-5 times the shear velocity). Flow augmentation (60% increase in flow speed relative to incident flow) was observed only above the homogeneously dense canopy, indicating development of a shear layer above the canopy. Quadrant analysis revealed that turbulent patterns observed in the vicinity of the homogeneous dense canopy were relatively orderly as compared to the sparse, moderately dense, and dense clustered canopies. Study findings quantify hydrodynamic variability found within natural intertidal oyster reefs, with applications to the design of reef-based natural infrastructure and prediction of how reefs may affect flow and sediment transport.

## ACKNOWLEDGMENTS

I would like to express my sincere gratitude to my advisor, Dr. Kelly Kibler, for her invaluable advice, guidance, and encouragement throughout the research process. Her expertise and mentorship, starting from day one of my research career, have been immensely beneficial, particularly during critical moments in the study. I am deeply appreciative of her support and constructive criticisms, which have helped me grow as a graduate student.

I am also indebted to my thesis committee members. Dr. Arvind Singh's teachings on Hydraulic Engineering and other water resources engineering modules have significantly enhanced my understanding of my research area. Dr. Thomas Wahl's teaching on coastal systems has provided me with a broader perspective on the subject. I am also grateful to Dr. Melinda Donnelly for accepting my invitation to join my thesis committee and for her guidance in shaping my career as a researcher.

I extend my heartfelt thanks to my fellow lab-mates, Sankar Mathavan, Peter Vien, and Jyotismita Taye, for their unwavering support throughout the research and data collection process. Their willingness to assist me, even in my absence during fieldwork, has been invaluable. Special appreciation goes to Joyce Salcedo Vera for her dedication to processing and analyzing sediment samples. I am deeply grateful to my former undergraduate research supervisor, Prof. Priyankara Perera, for setting my roots in research and providing guidance that paved the way for my higher studies. I would like to express my sincere appreciation to DARPA and NSF for providing financial assistance to carry out this research.

Finally, I would like to extend my utmost gratitude to my parents, sister, and brother-in-law for their unwavering support and belief in my dreams. Their encouragement and presence have been a constant source of strength. This achievement would not have been possible without their love and support.

Thank you.

# TABLE OF CONTENTS

LIST OF FIGURES.....	vii
LIST OF TABLES .....	ix
CHAPTER ONE: INTRODUCTION.....	1
Background of the Study.....	1
CHAPTER TWO: LITERATURE REVIEW .....	4
Oyster Reef Ecology and Dynamics .....	4
Habitat Preferences and Growth Dynamics.....	4
Reef Structure and Live Oyster Density .....	7
Oyster Reef Characteristics: Morphology and Classification .....	8
Oyster Reef Classification.....	8
Reef Rugosity .....	9
Hydrodynamic and Structural Characteristics of Oyster Reefs .....	10
Flow Velocity and Wave Attenuation .....	10
Turbulence Observed in Vicinity of Oyster Reef .....	11
Roughness and Drag Coefficient .....	13
Sediment Deposition.....	13
Problem Statement and Significance of the Study.....	15
Research Motivation and Objectives .....	16
CHAPTER THREE: METHODS .....	17
Study Location.....	17
Canopy Classification and Site Selection.....	18
Hydrodynamic Data Collection.....	20
Data Analysis .....	22
Mean Flows and Flow Attenuation: .....	23

Turbulent Fluctuations .....	24
CHAPTER FOUR: RESULTS .....	30
Reef-scale Hydrodynamics .....	30
Current Direction and Magnitude .....	32
Canopy-scale Hydrodynamics .....	36
Velocity Attenuation .....	36
Turbulence Production and Dissipation .....	38
Turbulence Intensity .....	44
Drag Coefficient.....	47
Quadrant Analysis .....	49
Sediment Analysis .....	56
CHAPTER FIVE: DISCUSSION.....	57
General Parameters Analysis.....	57
Flow Attenuation.....	59
Turbulence Intensities:.....	61
Drag Coefficient:.....	63
Turbulent Dissipation and Production: .....	65
Quadrant Analysis: .....	68
Conclusion.....	70
Future Work .....	72
APPENDIX: REEF LASER SCAN ANALYSIS FOR CANOPY HEIGHT .....	73
LIST OF REFERENCES .....	74

## LIST OF FIGURES

Figure 1. Eastern Oyster Reef in Mosquito Lagoon, illustrating distinctive heterogenous cluster arrangements.....	3
Figure 2. Study location in Mosquito Lagoon and locations of velocity data collection.....	18
Figure 3. Canopy Configurations within the reef: a) Sparse Canopy, b) Moderately Dense canopy, c) Dense canopy, d) Dense Homogenous canopy. ....	20
Figure 4. Position of instruments above and within the oyster canopy.....	21
Figure 5. Water level projection using elevation difference. $h$ is measured water depth, $E1$ and $E2$ are measured ground surface elevation, $h2$ is depth projected above. ....	23
Figure 6. Wind speed and direction recorded during seasonal a) high and b) low water levels. ....	31
Figure 7. Channel depth variation during high (H) and low (L) water level measurements. ....	32
Figure 8. Stream flow directionality within and above the canopy at: a) low water level, b) high water levels. ....	33
Figure 9. Boxplots of current speed observed during at low water levels a) within and b) above the canopy, and at high water levels c) within and d) above the canopy. Note the different y-axis scaling in part d.....	34
Figure 10. Mean flows incident to the reef and above and within the canopy during a) low water levels and b) high water levels. ....	35
Figure 11. Velocity attenuation from incident to canopy flows by canopy density during low water levels a) above and b) within the canopy, and during high water levels c) above and d) within the canopy. The black dashed 1:1 line represents no change in velocity.....	37
Figure 12. Mean velocity attenuation relative to channel and incident flows during low water levels a) within and b) above the canopy, and during high water levels c) within and d) above the canopy.....	38
Figure 13. Turbulence dissipation and production time series within and above the canopy during high and low water levels: a-b) SPA, c-d) MOD, e-f) DEN, g) H-DEN.....	40
Figure 14. Mean turbulence production and dissipation (a, c & e) and ratios of production to dissipation (b, d & f). ....	43
Figure 15. Turbulence intensity in all the canopies based on water levels: a) Considering full depth profile stream flow direction, b) Vertical direction c) Cross channel direction. ....	45
Figure 16. Mean normalized turbulence intensities across different canopy densities: a) Low water level, b) High water level. ....	46

Figure 17. Variability of drag coefficients observed during high water level above and within canopies of varying density: a-b) SPA canopy, c-d) MOD canopy, e-f) DEN canopy, g-h) H-DEN canopy. ....	48
Figure 18. Comparison across canopy density of a) mean drag coefficients within and above canopy and b) ratio between within- and above-canopy mean drag coefficients. ....	49
Figure 19. Quadrant analysis for SPA canopy observed during low water levels a) within and b) Low above the canopy and during high water levels c) within and d) above the canopy.....	50
Figure 20. Quadrant analysis for MOD canopy observed during low water levels a) within and b) above the canopy and during high water levels c) within and d) above the canopy.....	51
Figure 21. Quadrant analysis for DEN canopy observed during low water levels a) within and b) above the canopy and during high water levels c) within and d) above the canopy.....	52
Figure 22. Quadrant analysis for H-DEN canopy observed during high water levels a) within and b) above the canopy.....	53
Figure 23. Combined quadrant plots for all the canopy types considering high water level and canopy position: a) SPA canopy, b) MOD canopy, c) DEN canopy, d) H-DEN Canopy.....	54
Figure 24. Variation in reef sediment characteristics: a) sediment core sample transect, b) grain size distribution, c) organic matter content, d) uniformity coefficient relevant to each bulk core sample.....	56
Figure 25. Distance from incident flow to canopy locations.....	59
Figure 26. Development of boundary layer within the canopy types: a) SPA canopy, b) MOD canopy, c) DEN canopy, d) H-DEN canopy. ....	61
Figure 27. Evolutionary Traits in Oyster Reef Canopies. Comparison of canopy drag values illustrates how the MOD canopy exhibits traits of the SPA canopy, while the DEN and H-DEN canopies inherit characteristics from the MOD canopy.....	64
Figure 28. Canopy types divided into distinct regions based on the behavior of turbulence intensity, dissipation, and production values: a) SPA canopy, b) MOD canopy, c) DEN canopy, d) H DEN canopy.....	68
Figure 29. Laser Scan Analysis for Study site. ....	73

## LIST OF TABLES

Table 1. Relative wind speed and direction recorded with respect to SPA high and low water. ....	31
Table 2. Within- and above-canopy flow statistics with flow direction change shown relative to the channel flow direction. ....	35
Table 3. Reynold stresses Distribution among the quadrants for High water level. ....	55
Table 4. Reynold stresses Distribution among the quadrants for Low water level. ....	55

# CHAPTER ONE: INTRODUCTION

## Background of the Study

In the intricate tapestry of aquatic ecosystems, oysters emerge as pivotal players: they are ecosystem engineers that alter the natural environment and provide resources to other species (Jones et al., 1994). They form complex reef structures that provide ideal breeding grounds for fish, invertebrates, and other aquatic species (Lenihan & Peterson, 1998). Beyond their role as providers of habitat, oysters influence environmental quality through filter-feeding mechanisms of water filtration, which serves to enhance overall water clarity and quality (Dame et al., 1989). Additionally, oysters are capable of sequestering carbon, aiding in mitigating climate change.

Over the last few decades, the majority of the world's population has settled in coastal areas, and this trend is expected to persist in the future (Small & Nicholls, 2003). This global demographic shift has led to an increase in anthropogenic activities in coastal environments, while simultaneously exposing these areas to heightened flood risks and storms intensified by rising sea levels (Borsje et al., 2011; Donnelly et al., 2004). Consequently, the imperative for coastal protection through sustainable shoreline protection systems, such as natural barriers and eco-friendly engineering solutions, is now more critical than ever (Borsje et al., 2011; Temmerman et al., 2013).

Furthermore, their reef structures can be referred to as nature's breakwater, attenuating waves and stabilizing shorelines due to their ability to withstand hydrodynamic forces and grow reefs in pace with sea-level rise (Bouma et al., 2014). By mimicking nature, many sustainable approaches have been developed to address coastal erosion and flooding. The living shoreline concept is one example of adapting natural elements such as seagrass and oyster reefs to provide structural support to shorelines instead of conventional hard shoreline protection methods (Bilkovic et al., 2016). Nonetheless, the success rates of

these types of projects are still hindered due to a lack of in-depth knowledge. Therefore, it is important to study these nature's engineers as it will benefit mankind in coming up with solutions to tackle climate change and sea-level rise. Central to this inquiry, this research study focuses on eastern oysters (*Crassostrea virginica*) and understanding how the canopy condition of reefs influence flow hydrodynamics.

Spanning the waters of the Gulf of Mexico and the Atlantic Ocean, eastern oysters are resilient and adaptable, their life cycle closely connected with the ebb and flow of coastal environments. Oyster spawning occurs when they encounter adequate salinity and temperature conditions (Kraeuter et al., 2007; Shumway, 1996), and oyster larvae usually attach to hard substrates such as seawalls, mangrove prop roots, or existing oyster shells. Once attached, they start developing shells, and as they continue to settle and reproduce, they form complex structures called reefs. In a reef, oysters cluster together with a cement-like bond, varying spatially throughout the reef with different heights, density levels, and orientations (Fig. 1). Despite their importance, quantifying the extent and dynamics of oyster reefs has posed a formidable challenge to researchers due to the structural complexity within reefs. Hogan and Reidenbach used remote sensing methods employing Light Detection and Ranging (LiDAR) technology to determine the physical characteristics of oyster reefs (Hogan & Reidenbach, 2019). Cannon et al. (2023) utilized 3D laser scanning methods to map the surface of oyster reefs.

Building upon the foundational understanding established in the preceding discussion, the forthcoming literature review chapter delves deep into past research activities focused on oyster reefs. By analyzing the breadth and depth of studies examining oyster reef ecology, this review aims to uncover evolving insights into oyster reef dynamics and characteristics. Through a comprehensive analysis of seminal studies and contemporary research findings, it seeks to identify gaps, challenges, and opportunities for future investigation, thereby formulation of research questions that will guide the subsequent sections of this study.



Figure 1. Eastern Oyster Reef in Mosquito Lagoon, illustrating distinctive heterogenous cluster arrangements.

## **CHAPTER TWO: LITERATURE REVIEW**

This chapter provides a comprehensive overview of oyster reefs and their influence on flow parameters, crucial for shaping and refining the research objectives and hypotheses. The first section offers an overview of the physical and biological attributes of oyster reefs. It discusses the geomorphological formations and ecological features that shape oyster habitat preferences and growth dynamics, drawing on insights from seminal studies in the field. In the subsequent section, the focus reaches into the arrangement and dynamic processes within oyster reefs. It explores how factors such as reef structure, spatial distribution, and ecological interactions influence reef dynamics, incorporating findings from observational and experimental research. Transitioning from the discussion on arrangement and dynamics, the section on "Oyster Reef Characteristics: Morphology and Classification" examines the physical morphology and classification systems of oyster reefs. It reviews historical classifications proposed by researchers and presents contemporary approaches to categorizing oyster reef structures, highlighting the importance of intra-reef variations in understanding reef ecology. Finally, the section focusing on the interplay between hydrodynamics and reef structure investigates how flow patterns and structural attributes shape oyster reef ecosystems. It synthesizes findings from field measurements, and experimental studies to explain the hydraulic processes governing sediment transport, larval dispersal, and reef stability.

### **Oyster Reef Ecology and Dynamics**

#### **Habitat Preferences and Growth Dynamics**

Oysters are known to form dense vertical clusters that rise above the surrounding soft sediment, thus creating reefs (Bertness et al., 1998; Coen et al., 1999). However, the growth and structure of these reefs can vary considerably across habitats and geographical ranges. Eastern oyster reefs may exhibit as intertidal or subtidal fringing or patch reefs, ranging from small patches to expansive areas (Burrell, 1986; Coen et al., 1999; Kennedy et al., 1996; Mackenzie, 1983, 1996) Research suggests that oysters are most

abundant in areas offering partial predation refuge, such as low-salinity waters (< 15 ppt) or intertidal zones, with water temperature and salinity positively correlated with oyster growth (Kraeuter et al., 2007; Shumway, 1996). However, high air temperatures can pose a threat to intertidal oysters (Byers et al., 2015a; Malek & Breitburg, 2010).

Regarding the relationship between inundation time and reef dynamics, longer inundation durations on a reef extend oyster submergence, thereby prolonging feeding and enhancing growth (Bahr, 1976; Bartol et al. 1999; Roegner & Mann, 1995). Nonetheless, increased submergence time does not unilaterally lead to higher growth rates, as other factors like reduced desiccation stress also play a role (Crosby et al., 1991; Peterson & Black, 1988). Prolonged submersion can even have adverse effects on oyster survival, with subtidal oysters experiencing higher rates of predation and biofouling compared to intertidal counterparts (Byers et al., 2015b; Fodrie et al., 2014).

When considering reef base and substrate construction, it is crucial to mimic the vertical relief and interstitial space provided by mounded oyster shells to ensure viable oyster populations and the coexistence of natural reef communities (Drexler et al., 2014). Research indicates significant variations in oyster density among habitats such as artificial substrates (e.g., seawalls), mangroves, and natural reefs, with natural reefs exhibiting the lowest mean density but the highest shell heights ( $37.9 \pm 14.6$  mm) and lowest biomass ( $289 \text{ g/m}^2$ ), followed by mangroves ( $32.1 \text{ mm} \pm 13.8 \text{ mm}$ ,  $346 \text{ g/m}^2$ ) and seawalls ( $33.4 \text{ mm} \pm 13.8 \text{ mm}$ ,  $507 \text{ g/m}^2$ ) (Bobo et al., 1997; Brown et al., 2005; Drexler et al., 2014). This suggests that oysters prefer a distributed arrangement with sufficient substrate space for attachment, while substrate size and exposure time during tidal cycles significantly influence shell growth. Additionally, oysters from natural reefs exhibit higher resilience against parasitic infections like *Perkinsus marinus*, likely due to prolonged submergence during tidal cycles, increasing the risk of disease invasion in reef habitats and thereby favoring the prevalence of reef-based oysters (Bobo et al., 1997; Brown et al., 2005; Drexler et al., 2014).

The arrangement of oyster reefs is influenced by various factors, including the location of the reef (subtidal or intertidal), oyster species, and water level conditions such as salinity. When considering the structure of an oyster reef, it primarily comprises biogenic sediment from oysters, including skeletal shell material and bio deposits (feces and pseudo feces), along with sediment from shoreline erosion and resuspension (Bahr & Lanier, 1981; Grabowski et al., 2005; Hargis, 1999; River et al., 1988).

Reef structure is governed by reef accretion and erosion rates. Reef accretion involves oyster shell production, bio deposition, and allogenic sediment, while reef erosion entails bioerosion, predation, and dissolution. Research conducted by Rodriguez et al. (2014) on eastern oysters at the Coastal Marine Research Reserve in North Carolina revealed that higher growth rates can be expected on newly constructed intertidal oyster reefs (1-2 years old) compared to older intertidal reefs (close to 10 years old). Initially, all oyster reefs were constructed at approximately the same elevation below sea level. Oyster reefs rapidly increase in height during the first few years, with growth rates declining as reefs approach the upper limit of the tidal range due to heightened stress from limited inundation. Vertical accretion of the reef crest is mainly driven by the need for refuge from biofouling, predation, and diseases. Intertidal oyster reefs, in particular, provide more conducive environmental conditions for oyster growth. Experimental evidence indicates that intertidal reefs grow 34% faster than subtidal oysters and attract fewer marine organisms, resulting in less fouling (Bishop & Peterson, 2006). This provides more space for oyster larvae settlement. Rodriguez et al. (2014) further explains that the growth of the oyster reef will be halted when it reached to the upper limit of the tidal range.

Regarding suitable locations for oyster reefs, research by Salvador de Paiva et al. (2018) on Pacific oyster reefs in the Netherlands found a positive correlation between active or growing reefs and eroding tidal flats, with a negative correlation observed on accreting tidal flats. This suggests that when an oyster reef is located adjacent to accreting tidal flats, they are more prone to burial from sediments, resulting in higher mortality rates. Hence, the surrounding environment directly interacts with reef development.

Additionally, studies by Bahr & Lanier, (1981) and Grizzle, (1990) highlighted the significant impact of physical variables such as tidal ranges on individual reef size and overall areal coverage within an estuary. Salvador de Paiva et al. (2018), highlights that the shape of the tidal flat where the oyster reef is located affects its development, with larger elevation changes found in convex tidal flats than concave ones. Authors further noted that more protuberant or sunken reefs are more likely to experience high growth, as tidal flats subjected to erosion tend to be submerged in water for longer durations than concave reefs.

### **Reef Structure and Live Oyster Density**

Oyster reefs represent distinct ecosystems that exert significant physical and biological influence on estuaries. Physically, they act as natural filters, removing suspended particulate matter (Newell, 1988) and altering current patterns (Lenihan, 1999b). Biologically, they play a crucial role in phytoplankton removal and contribute to the production of substantial oyster biomass (Dame & Patten, 1981). Characterized by unique geomorphological features, oyster reefs typically exhibit lower slopes compared to adjacent sand bars or tidal flats. Research by Cannon et al. (2022) conducted in Mosquito Lagoon, Florida, revealed that both natural and successfully restored oyster reefs in this region have slopes ranging from 6% to 18%.

When examining oyster canopy dynamics, it becomes evident that oysters on natural reefs form vertically oriented clusters that extend above the reef bed, creating a roughness sublayer significantly larger than that of mud and sand substrates (Cannon et al., 2022; Stiner & Walters, 2008; Styles, 2015). Cannon et al. (2023) further investigated eastern oyster canopy characteristics, observing variations in average canopy height varied from 36 mm to 49 mm and live oyster shell length varied from 37.6 mm to 58.8 mm across restored and natural reefs in Mosquito Lagoon, Florida. Similarly, Walters et al. (2020) reported comparable mean shell heights ( $46.3 \pm 1.4$  mm) for restored eastern oyster reefs in Mosquito Lagoon six months after deployment( Cannon et al., 2023).

In terms of oyster density, Walters et al. (2020) observed approximately 922-1053 oysters per square meter in a set of restored reefs in Mosquito Lagoon. Additionally, Ridge et al. (2015) and Grizzle et al. (2018) documented an overall mean live eastern oyster density of 1383 individuals per square meter, with a mean shell height of 46.5 mm, in the Rachel Carson Reserve, North Carolina, and its nearby coastal environment.

### **Oyster Reef Characteristics: Morphology and Classification**

Grave, (1905); Price, (1954); and Smith et al. (2003) delineate three distinct oyster reef morphologies: string reefs, fringe reefs, and patch reefs. String reefs, characterized by elongated form perpendicular to tidal flow, exhibit heightened productivity and a prominent vertical structure, as documented by Woods et al. (2005). Conversely, fringe reefs, narrow formations located along tidal channels, display a lower vertical profile and a shorter lifespan compared to string reefs (Smith et al., 2003). While fringe reefs serve as optimal settling grounds for oyster larvae due to the proximity to tidal currents, their reef crests are vulnerable to sediment burial due to low sediment resuspension. The elevation of relief significantly influences reef growth dynamics, with Colden et al. (2016) highlighting higher oyster survival rates on crests of tall reefs with faster flow speeds ( $\geq 0.1$  m reef height), attributed to reduced sediment deposition and increased particulate flux while, oyster mortality is greatest at bases of reefs with low vertical relief (0.1 m) due to sedimentation. Colden et al. (2016) conducted field experiments to assess the hydrodynamic and sediment dynamic implications of reef orientation, finding that reef oriented perpendicular to flow demonstrate greater longevity and stability over time. Moreover, sediment surrounding perpendicular reefs exhibits finer characteristics compared to parallel and circular reefs.

### **Oyster Reef Classification**

Despite the significance of oyster reefs, there exists no universally accepted classification system for oyster reefs. Smaal et al. (2009) introduced one such classification, defining oyster reefs as clusters of oysters

with a minimum diameter of 50 cm, located within proximity to other oyster patches, with a maximum distance of 10 m between them. However, this classification overlooks intra-reef variations. In an effort to address this gap, Hitzegrad et al. (2022) proposed a more comprehensive intra-reef classification system. Utilizing high-resolution Digital Elevation Models (DEM) and Structure-from-Motion (SFM) photogrammetry, they developed this classification based on visual observations in the field and statistical analyses of bed topography. Their proposed system includes seven structural classifications, such as Central Reef, Transitional Zone, Cluster I, Cluster II, Patch I, Patch II, and Garland, based on observations of *Magallana gigas* oyster reefs in the Central Wadden Sea, Germany. The authors suggest that such intra-reef classification allows for a more nuanced understanding of hydraulic processes, sediment transport dynamics, and larval distribution within oyster reefs.

### **Reef Rugosity**

Reef rugosity is closely linked with reef building, as it promotes sediment trapping by reducing shear stress on sediments (Rodriguez et al., 2014). Reef rugosity serves as a critical index for assessing the structural complexity of biological formations, providing insight into their intricate arrangements. Initially proposed by Michael Risk in 1972, rugosity quantifies complexity by comparing the actual length of a surface to its straight or horizontal length over a specified distance (Michael Risk, 1972). While this method is cost-effective and straightforward, it may not capture the precise structural intricacies present on a reef. Oyster reefs, for instance, exhibit varying rugosities across their formations due to the arrangement of different cluster types, resulting in varied hydrodynamic flow patterns throughout the reef. Understanding these precise rugosity variations is crucial for comprehending full-scale flow dynamics. Cannon et al., (2023) utilized 3D interpolation of point cloud data obtained from laser scans of eastern oyster reefs, creating a  $0.5 \times 0.5$  grid to estimate reef rugosity. By defining the total irregular surface area divided by the bed area beneath the canopy, they observed rugosity ranging from 1.28 to 1.56 across three restored reefs and one natural reef in Mosquito Lagoon. Additionally, they measured the fractal dimension of the reef

canopy, reflecting canopy complexity, which ranged between 2.67 and 2.74. The fractal dimension is a concept that measures the complexity and irregularity of a structure and is strongly correlated with human visual perception of roughness (Pentland, 1984). It varies from 2 to 3 for three-dimensional surfaces, with values closer to 3 representing more complex surfaces (Cannon et al., 2023).

### **Hydrodynamic and Structural Characteristics of Oyster Reefs**

In the previous section, past research findings were explored regarding the identification of the structure of oyster reefs, canopy ecology, and habitat preferences. This section shifts the focus to research findings on oyster reefs, with a particular focus on their influence on hydrodynamics and manipulation, as well as canopy roughness parameters affecting these dynamics.

#### **Flow Velocity and Wave Attenuation**

When focusing on flow velocity and wave attenuation, Wiberg et al. (2019) observed a significant reduction in wave heights within the intermediate water depth range, approximately several 10 cm below and above the reef crest, in a study conducted in Ramshorn Bay and South Bay, Virginia. However, the impact of reefs on wave height was less pronounced at higher water depths. The greatest change in wave height across the reef was noted when the water depth was within  $\pm 0.25$  m of the reef crest elevation. Similarly, Cannon et al. (2022) observed an average attenuation of 25% when comparing waves in a channel to waves encountering a reef. However, during this study, all restored, and reference reefs were submerged by water. In terms of flow velocity, it undergoes attenuation when flowing over a rough surface due to skin friction and form drag forces created by the roughness, resulting in increased shear forces and turbulence, thereby reducing velocity. On smooth surfaces, flow tends to exhibit laminar flow and higher velocities. Styles (2015) observed this phenomenon when measuring flow velocity over sand banks and oyster banks. Similarly, Kitsikoudis et al. (2020) measured mean flow velocity over degraded and living

oyster reefs, noting lower mean flow values over living reefs compared to degraded reefs. This suggests that mean flow velocity can serve as a measurement parameter for oyster reef enhancement efforts.

Furthermore, Cannon et al. (2022) measured flow velocities at two profiles: above (9.5 cm) and within (2 cm) the canopy, observing 84%-97% velocity attenuation with respect to channel flow near the bed and 51%-65% attenuation above the canopy. These findings underscore the role of oyster reefs in altering flow dynamics and wave characteristics within their vicinity, highlighting their significance in coastal protection and habitat enhancement efforts.

### **Turbulence Observed in Vicinity of Oyster Reef**

Numerous studies have underscored the importance of turbulence around oyster canopies in creating favorable hydrodynamic conditions for oysters. Dame (1996) suggests that flow-induced instabilities around the rigid shell of oysters lead to eddy shedding and turbulence generation, thereby enhancing mixing and dispersion. Similarly, researches by Chang & Constantinescu (2015), Fuchs et al. (2013), Hubbard & Reidenbach (2015) and Kitsikoudis et al. (2016) indicate that oyster clusters within the flow convert flow kinetic energy into turbulence, serving as a cue for oyster larvae. Turbulence on an oyster reef can primarily result from two phenomena: bed-generated turbulence and turbulence due to eddies shed from oysters (Kitsikoudis et al. 2020). The presence of elevated turbulence can lead to higher energy events on an oyster reef. Sumer et al. (2003) suggest that elevated turbulence can increase sediment transport rates, while Yang et al. (2016) confirm greater rates of sediment flux under elevated turbulence within simulated vegetation canopies.

Styles (2015) further builds on these findings, suggesting that oysters tend to cluster near areas favorable for turbulent eddy formation, as eddies trap particles and increase residence time. Reynolds stress, a measure of turbulent momentum transport in a flow field, was found to be higher over oyster reefs compared to sand banks in studies conducted by Styles (2015), with maximum Reynolds stress reaching

22  $\text{cm}^2\text{s}^{-2}$  over oyster reefs compared to 6  $\text{cm}^2\text{s}^{-2}$  over sand banks. Additionally, higher Reynolds stress was observed along the channel of the oyster reef compared to cross-channel stress.

Turbulence generally scales with local velocity, with higher velocities associated with enhanced mixing rates. Cannon et al. (2022) observed the highest mixing rates above the oyster canopy, with mean vertical turbulent energy dissipation and turbulent shear production estimates ranging from  $10^{-4} \text{ m}^2\text{s}^{-3}$  to  $10^{-3} \text{ m}^2\text{s}^{-3}$  and  $10^{-5} \text{ m}^2\text{s}^{-3}$  to  $10^{-4} \text{ m}^2\text{s}^{-3}$  respectively. Cannon et al. (2022) further observed that turbulence characteristics within the canopy of restored reefs were more variable compared to above the canopy with turbulent shear production ( $P$ ) being on average, 3–4 times greater than turbulent dissipation ( $\varepsilon$ ) for the above canopy.

However, Kitsikoudis et al. (2020) observed that the turbulence dissipation and production rates were on the order of magnitude of  $10^{-4} \text{ m}^2\text{s}^{-3}$  and within the canopy (1 cm), the dissipation rate was lower than the production rate in reference and degraded reefs. Above the canopy of reference reefs (5 cm), they observed a more balanced pattern between turbulence production and dissipation. However, these values were lower than the dissipation values recorded by Styles (2015), who observed dissipation rates varying from  $10^{-4} \text{ m}^2\text{s}^{-3}$  to  $10^{-3} \text{ m}^2\text{s}^{-3}$ , aligning with the dissipation rates observed by Cannon et al. (2022)

Furthermore, in a review of dissipation rates in other aquatic canopies besides oyster reefs, Reidenbach et al. (2006) observed dissipation rates ranging from  $10^{-6} \text{ m}^2\text{s}^{-3}$  to  $10^{-5} \text{ m}^2\text{s}^{-3}$  at 10 cm above fringe coral reefs. Similarly, Kibler et al. (2019) noted dissipation rates on the order of magnitude of  $10^{-5} \text{ m}^2\text{s}^{-3}$  and  $10^{-6} \text{ m}^2\text{s}^{-3}$  for flows through mangroves and emergent marsh grass, respectively. Additionally, Pieterse et al. (2015) observed dissipation rates on the order of magnitude of  $10^{-3} \text{ m}^2\text{s}^{-3}$  near the bed of a tidal channel in a salt marsh. The varying values for dissipation rates can be attributed to the complex nature of aquatic canopies, including differences in canopy characteristics and dissipation rate measurement distances and methods.

These findings collectively underscore the complex interplay between canopy structure and turbulence dynamics, highlighting the importance of turbulence in shaping ecosystems.

### **Roughness and Drag Coefficient**

Styles (2015) calculated the drag coefficient ( $C_d$ ) on oyster reefs located in North Inlet Estuary, South Carolina using the quadratic drag law method, which relates Reynolds stress to mean flow. Additionally, Styles (2015) computed the hydraulic roughness ( $z_0$ ) based on the drag coefficient. From the results, he reported that the  $C_d$  and  $z_0$  over oyster banks are an order of magnitude higher than those over sand banks ( $C_d$  Oyster reef = 0.0174-0.0322 /  $C_d$  Sand = 0.0036-0.0048). Similarly, Wright et al. (1990) observed drag coefficients, friction velocity, and roughness estimates of 0.008, 3-8.5  $\text{cm s}^{-1}$ , and 1 cm over oyster beds using the log profile technique. Furthermore, Whitman & Reidenbach, (2012) measured turbulence quantities over oysters and reported a drag coefficient of 0.019 and a hydraulic roughness of 1.7 cm. They further stated that increased bed roughness is beneficial for larval recruitment, and vertically oriented roughness elements create interstitial regions that aid in larval recruitment and provide shelter against high velocity and bed shear stress. Kitsikoudis et al. (2020) also measured the drag coefficient on natural reefs and observed a mean of approximately 0.031, higher than that observed by Whitman & Reidenbach, (2012). This disparity is mainly attributed to the measurement location, as Whitman & Reidenbach, (2012) estimated  $C_d$  40 cm above the oyster reef with a vertical offset, while Kitsikoudis et al. (2020) and Styles, (2015) measured drag forces 1 cm and 10 cm from the bed, respectively. Additionally, research by Bartol & Mann, (1999) observed that the complex three-dimensional structure created by years of successive settlement on oyster reefs provides physical and biological refugia for oysters.

### **Sediment Deposition**

The suspension feeding mechanism of oysters plays a crucial role in filtering organic, inorganic, and particulate matter from the water column, as documented by Nelson et al. (2004) and Newell (1988). Base

on the scientific finding eastern oysters can clean approximately over 100 liters of water per day per individual, while pseudo feces deposited by oysters can amount to one to two times the oyster's dry tissue weight per week (Haven & Morales-Alamo, 1966), significantly increasing particle settling rates compared to normal gravity deposition (Dame, 1999). Flow velocity directly influences sediment deposition and erosion dynamics. Reidenbach et al. (2013) conducted field experiments on intertidal oyster reefs along the Virginia coastline, revealing a positive correlation between sediment fluxes to the benthos and mean flow velocities below  $10 \text{ cm s}^{-1}$ . Sediment suspension decreases and erosion initiates at velocities exceeding  $10\text{-}15 \text{ cm s}^{-1}$ , consistent with findings by Dame et al. (1985). Kitsikoudis et al. (2020) observed a higher fraction of fine sediment in reference oyster reefs with elevated turbulence and kinetic energy due to canopy density compared to degraded reefs with low turbulence mixing.

High sedimentation rates can adversely affect oyster recruitment, with larvae and adult oysters at risk of burial, thus impeding recruitment and growth (Mackenzie, 1983). Lenihan, (1999) noted that sedimentation was seasonally highest at the bases of the reefs, resulting in greater mortality compared to oysters on the reef crest. Similar patterns were observed by Reidenbach (2012), who found lower suspended sediment concentrations at higher elevations on eastern oyster reefs. These findings suggest that the physical structure and location of the habitat can notably influence the growth and survival of oyster communities.

## **Problem Statement and Significance of the Study**

In light of the insights gained from the extensive review of past research on oyster reefs, it has been noted that eastern oysters present a unique structural arrangement that varies spatially and influences flow hydrodynamics within their habitat. The surface of natural oyster reefs forms vertically oriented clusters with uni- or multi-directional arrangements, protruding into the water column and creating roughness several orders of magnitude larger than the roughness height of mud or sand (Cannon et al., 2022; Stiner & Walters, 2008; Styles, 2015). The density of these clustered oyster shells varies across the reef, resulting in diverse canopy densities throughout. While previous hydrodynamic research has predominantly treated oyster reefs as singular systems, measuring hydrodynamic parameters accordingly, the reality is that oyster reefs can be further subdivided into subsystems based on variations in oyster canopy cluster arrangements. This study primarily aims to identify how these different canopy densities influence flow dynamics and understand how these subsystems contribute to overall reef hydrodynamics.

The significance of this research study lies in its potential to address the critical gap in our understanding of reef hydrodynamics. It aims to bridge the knowledge divide between the overall reef hydrodynamic of reef system and their subsystem level contribution with a focus on the canopy density. Further this research gives a new perspective of looking at reef hydrodynamic in a micro scale point of view, that help to understand the to capture intricate hydrodynamic information that will be beneficial in ecosystem restoration and conservation of oyster reefs. Moreover, this study leads the path to understand other scientific parameters such as sediment transport, nutrient transport etc. in the point of view of subsystem levels.

## **Research Motivation and Objectives**

The research is designed as an experimental investigation to identify the hydrodynamic variability of flow within an oyster reef. While researchers have studied flow in the vicinity of oyster reefs as a single system, none have investigated the spatial variability of flow changes within an oyster reef. Documenting the heterogeneity of flow within a single reef serves as the primary motivation behind the research study. The study hypothesizes that structure of the oyster canopy profoundly influences the local hydrodynamic environment such that considerable hydrodynamic variability may be present within a single reef. The author further posits that the hydrodynamic variability will not be random, but rather a systematic response to canopy configuration, such that specific and predictable hydrodynamic signatures may be found along a gradient of canopy densities, as well as within and above the oyster canopy. When designing natural living shoreline systems that include oyster reefs, it is crucial to base created habitats on the natural reef morphology and function. The reef condition as found in nature represents the natural design process, integrating evolutionary-scale processes to create dynamic equilibrium within coastal ecosystems. This study primarily focuses on capturing the micro-scale signature of flow within an oyster reef based on different cluster arrangements. The objectives of this study are thus to compare hydrodynamic parameters within a single oyster reef across varied canopy densities to assess the influence canopy variation to flow and propose a generalized classification oyster canopy from a hydrodynamic perspective.

## CHAPTER THREE: METHODS

### Study Location

A field investigation was conducted in Mosquito Lagoon, a microtidal estuary situated along the Atlantic coast of Florida, USA. Mosquito Lagoon, the northernmost region of the Indian River Lagoon system (IRL), is characterized by extensive development along shorelines in its northern half and limited development along southern shorelines connected to Canaveral National Seashore (CANA) and Merritt Island National Wildlife Refuge (Phlips et al., 2015). It is primarily dominated by semi-diurnal tidal currents (Smith, 1990) with seasonally varying water levels. The climatic conditions in Mosquito Lagoon are humid subtropical, with temperatures ranging from 25-30°C and salinity levels between 10-40 ppt (Down & Withrow, 1978). It has a mean water depth of 1.7 m and is characterized by wind-driven circulation. Additionally, it is subject to long water residence times and, more recently, high nutrient loadings (Smith, 1993; Steward et al., 2006). Mosquito Lagoon is home to various aquatic species and numerous intertidal eastern oyster reefs. One intertidal reef was selected for investigation (Fig. 2), primarily because local hydrodynamic processes were conducive to investigation. The study reef was situated amongst many other reefs in a shallow, protected bay created by permanent vegetated islands. Notably, the reef chosen for study was positioned directly downstream of a relatively narrow channel through which primary tidal exchange occurred, making it an ideal place to discern the reef impact to the incoming flow signature. The study reef also exhibited diverse variation in canopy density, which was necessary for this study. The patch reef area was approximately 2500 m<sup>2</sup>, consisting of an outer transition zone between the fully developed reef and the seafloor bed. The inner reef area was approximately 1450 m<sup>2</sup> consisting of reference condition, fully developed oyster canopy.

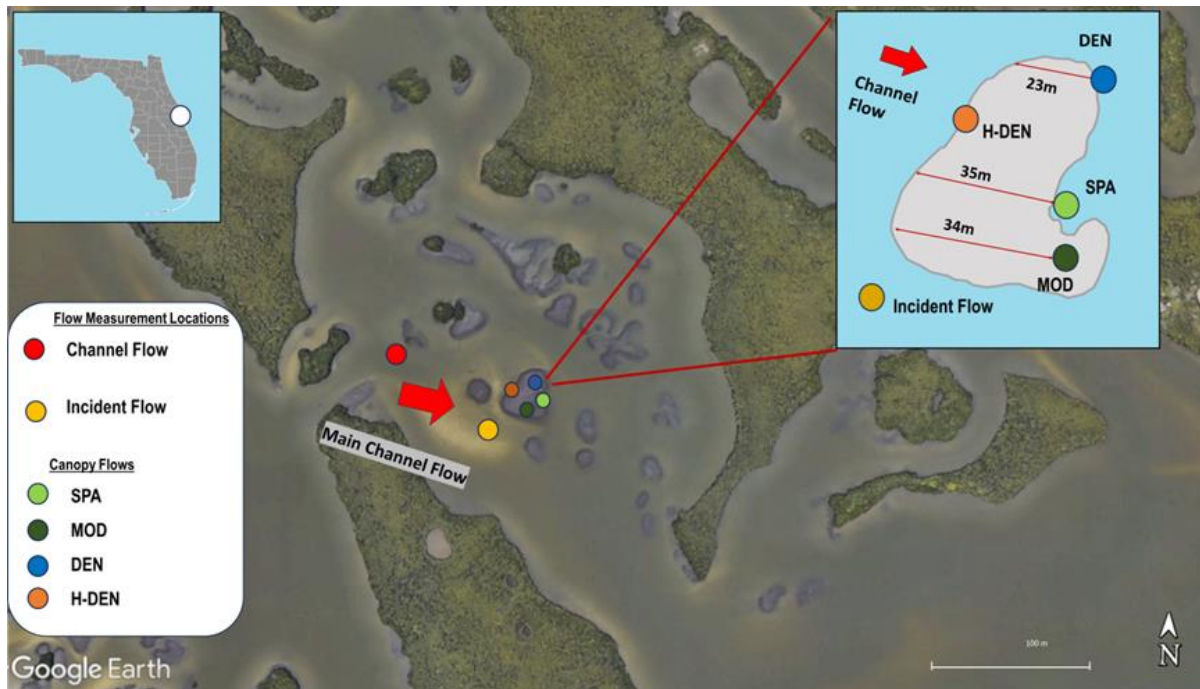


Figure 2. Study location in Mosquito Lagoon and locations of velocity data collection.

### Canopy Classification and Site Selection

Preliminary topographic and visual canopy classification surveys were conducted at the study reef. It was observed that the reef boundary areas were comprised of tightly clustered oysters with high elevation. Moving within the reef, the elevation became lower, and clusters of oysters were more widely distributed. Sites for hydrodynamic data collection were selected from diverse locations of the heterogeneous reef canopy. The reef canopy structure was classified using a methodology inspired Hitzegrad et al., (2022) by visual inspection during low water levels. The canopy was classified into Sparse (SPA), Moderately Dense (MOD), Dense Clustered (DEN), and Dense Homogeneous (H-DEN) categories (Fig. 3). Moreover, canopy height for each density type was obtained using the FARO x330 terrestrial high-resolution laser scanner, following the methodology outlined in Cannon et al. (2023)(Appendix). It was observed that MOD, DEN,

and H-DEN canopies had approximate heights of 2.7 cm, 4.3 cm, and 6.7 cm, respectively. Additionally, it was noted that SPA canopies lack vertical development.

The Sparse (SPA) canopy type was found primarily in the lowest elevations of the reef, where the reef side slope transitioned to the sandy channel bed (Fig. 3a) and was submerged even during low water levels. Typically located at the outer radius of the reef, this canopy was characterized by loose, disarticulated oyster shells, few live oysters, and bare sandy sediments. Live oysters were predominantly oriented horizontally, with few clustered oysters protruding vertically into the water column. The Moderately Dense (MOD) canopy (Fig. 3b) was found in the middle of the reef, characterized by vertically oriented clusters with moderate density. The arrangement and orientation of clusters were not homogeneous, but clustered, and disarticulated shell was present on the bed between clusters. No bare sediments were observed between the clusters. The middle of the reef exhibited a basin-like structure, with the central area depressed compared to the reef edges. As a result, the Moderately Dense canopy was subject to longer periods of inundation as compared to Dense (DEN) and Dense Homogeneous (H-DEN) canopy types, (Fig. 3c and d) which were found at the highest reef elevations. The Dense canopy types were situated at the outer edges of the reef and characterized by packed, vertically oriented formations. The Dense Homogeneous (H-DEN) canopy was found at the highest reef elevations and was inundated the least of any canopy type. The homogeneous canopy resembled cleanly cut grass, perfectly oriented vertically with uniform height and no space between individual oysters. The bed of disarticulated shells was hardly visible. The Dense Cluster (DEN) arrangement by contrast was non-homogeneous and clusters resembled a flower-like pattern around 360 degrees. Dense Clustered (DEN) canopies were located in areas with slightly lower elevation compared to Dense Homogeneous (H-DEN) canopies but at a higher elevation than Sparse (SPA) and Moderately Dense (MOD) canopy types.

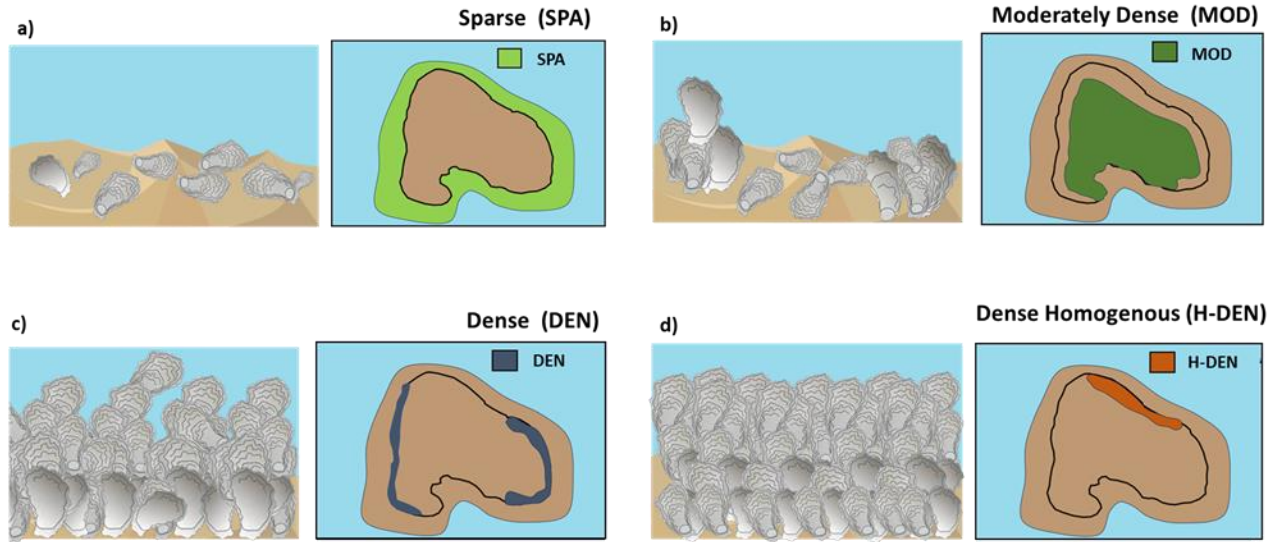


Figure 3. Canopy Configurations within the reef: a) Sparse Canopy, b) Moderately Dense canopy, c) Dense canopy, d) Dense Homogenous canopy.

### Hydrodynamic Data Collection

Flow transects were measured with acoustic velocimeters in the channel, incident to the reef and in various locations of the study reef canopy through flood tides during seasonal low and high water levels. All instruments were aligned to a common coordinate system and orientated toward 270°N facing the channel. The instruments were aligned to capture three-dimensional velocity components of the flow: the  $u$  velocity component along the main flow direction, the  $v$  velocity component along the cross-channel direction, and the  $w$  component in the vertical direction. Within the reef canopy, velocity profiles (each approximately 2.5 cm) were recorded using two Nortek Vectrino Profilers (Fig. 4), each with a 4 cm blanking distance and a sampling rate of 100 Hz. The profilers were positioned to record flow dynamics simultaneously near the bed (within the oyster canopy, profile midpoint 5 cm above bed) and above the canopy (profile midpoint 10 cm above bed, within 5 cm of the canopy top). The bottom distances (from the probe to bottom) were 10.5 cm and 15.5 cm, respectively.



Figure 4. Position of instruments above and within the oyster canopy.

Flow approaching the reef was recorded in the channel with a Nortek Aquadopp HR profiler. The HR Profiler was positioned facing up in the channel. It had a blanking distance of 10.1 cm and was initialized to measure flow velocity up to a depth of 86 cm. The profiler recorded velocity at a cell size of 20 mm and consisted of 43 cells. It sampled data in a burst mode, with continuous samples taken at 2 Hz frequency, and the interval between bursts was 6 hours. An Onset Hobo U20L Water level logger was positioned with the HR Profiler with a 5-minute interval for data collection. Both the HR Profiler and the water level logger were installed approximately 42 m from the nearest leading edge of the reef. Incoming flow incident to the reef was recorded with a Nortek Vector Profiler installed approximately 10 m from the leading edge of the reef. The Vector probe was installed 20 cm from the bottom to measure flow (32 Hz) at a point 5 cm above the bottom. A R.M. Young 05103L wind sensor was installed close to the study reef to record wind speed and direction at 1-minute intervals. Hydrodynamic data collection was repeated for each canopy density (SPA, MOD, DEN and H-DEN) when water levels were seasonally low (Spring) and high (Fall) to capture the range of variability in annual flows.

During low water levels, reef canopy height was manually characterized using quadrat sampling methods. Quadrats of 0.25 m<sup>2</sup> in size were centered around the Vectrino locations. Within each quadrat, every solid

element, including clustered shells or individual shell elements, was measured with Vernier calipers along both the vertical and largest horizontal axes. Sediment characteristics were assessed through a transect at the study reef. Seven bulk sediment cores (diameter: 7.2 cm) were collected, capturing transects from the channel bed just off the reef, two samples along the reef slopes, and four samples within the reef canopy. The sediment cores were extracted to a depth of approximately 15 cm, along with water trapped in the core tubing. Subsequently, sediment samples were oven-dried at 110°C for more than 24 hours, and particles were carefully manually separated. Organic matter content (OM) was evaluated for each core based on the mass lost on ignition (16 hours at 550°C) of 20 g samples of sand and finer sediments ( $D < 2$  mm). Cores from each location underwent separate particle size analysis, conducted using a combination of wet and dry sieve analysis to improve the accuracy of mass estimates for silt and clay sediments (ASTM, 2006, 2013).

### **Data Analysis**

The relevant wind data for the data collection period were extracted from the sensor and the wind speed distribution was plotted using a histogram to identify the frequency of different wind speed intervals for each day. Subsequently, wind rose diagrams were developed to visualize the distribution of wind directions and corresponding wind speeds for each day. Finally, a set of wind rose diagrams was developed to compare the wind characteristics during low water and high-water studies. Gauge pressure recorded by the water level logger difference was derived by subtracting the atmospheric pressure at the site from the measured absolute pressure. The water depth ( $h$ ) was determined using Equation 01 and 02, where  $\Delta P$  represented the pressure difference,  $\rho$  denoted water density,  $g$  was gravitational acceleration, and  $h$  signified water depth. Elevation points acquired through RTK surveying for both the channel and canopy locations were utilized to extrapolate water level data. The elevation discrepancy was computed to extend water level projections from the channel to all canopy locations (Fig. 5).

$$\Delta P = P_{abs} - P_{atm} \quad \text{Eq (01)}$$

$$\frac{\Delta p}{\rho g} = h \quad \text{Eq (02)}$$

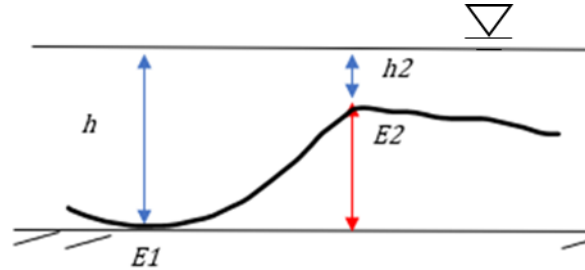


Figure 5. Water level projection using elevation difference.  $h$  is measured water depth,  $E1$  and  $E2$  are measured ground surface elevation,  $h2$  is depth projected above.

### Mean Flows and Flow Attenuation:

Velocity measurements underwent quality control by removing data with less than 20% Signal-to-Noise Ratio (SNR) and less than 75% correlation. Resultant gaps in the data were replaced by linear interpolation. The data relevant to exact data collection were obtained, with all disturbances discarded. All time series were despiked to remove further noise and anomalies using the phase thresholding algorithm (Goring & Nikora, 2002; Wahl, 2003). The mean velocity time series were calculated by averaging quality-controlled time series data over 120 seconds of sampling with a 50% overlap. Here, it was assumed that the flow was quasi-steady over 2-minute data segments. Streamwise velocity profiles ( $U$ ) (Eq 03) and their directionality (Eq 04) were calculated using quality-controlled and time-segmented mean  $\bar{u}$  and  $\bar{v}$  velocity components for each instrument station. The velocity attenuation calculation involved plotting canopy flow against both channel and incident flow velocities and fitting a linear trendline to the data. Subsequently, the deviation of the canopy flow from the channel flow and incident flow was determined by the departure of the slope of the least squares line from 1:1 line. Flow attenuation ( $A_s$ ) was calculated by subtracting the least square line slope from 1, as demonstrated in the equation Eq 05.

$$U = \sqrt{\bar{u}^2 + \bar{v}^2} \quad \text{Eq (03)}$$

$$\phi = \tan^{-1} \frac{\bar{v}}{\bar{u}} \quad \text{Eq (04)}$$

$$A_s = 1 - \text{slope of the least squares line} \quad \text{Eq (05)}$$

Here  $\bar{u}$  represents the mean flow velocity in the x-direction, and  $\bar{v}$  represents the mean flow velocity in the y-direction. Flow attenuation ( $A_s$ ) is defined as the one minus the ratio of flow within the canopy to the incident flow. Flow attenuation was calculated separately for each canopy type and position, considering both within- and above-canopy measurements. Additionally, the calculations were performed separately for both low- and high-water seasons.

### **Turbulent Fluctuations**

Flow measurements were decomposed to eliminate interference from waves before analyzing the fluctuating portion of the velocity timeseries. While the contribution from waves was observed to be minimal during the low water season, some contribution of waves was observed during the higher water measurements. Instantaneous velocity measurements captured from the flow measuring devices consist of wave oscillations ( $\tilde{u}_i$ ), turbulent fluctuations ( $u'_i$ ), that both deviate from the mean flow ( $\bar{u}$ ) as in Eq (06):

$$u_i = \tilde{u}_i + u'_i + \bar{u} \quad \text{Eq (06)}$$

Here  $u_i$  represent the instantaneous three-dimensional velocity vector ( $u, v, w$ ). For each 120s segmented velocity timeseries, the energy associated with mean flow ( $\bar{u}$ ), fluctuation associated with surface waves ( $\tilde{u}_i$ ), and turbulence ( $u'_i$ ) were separated using the phase separation method (Bricker & Monismith, 2007). After removing wave variation, analysis of turbulence was undertaken.

Reynolds stresses were calculated to characterize the intensity and direction of turbulent fluctuations. These stresses were employed to quantify the variation of turbulence intensities with depth ratio. The turbulent fluctuation component was derived from the wave-removed Reynold decomposition (above in Eq 06). When considering a homogeneous flow with density  $\rho$ , the Reynold stress tensor ( $\tau'_{ij}$ ) can be defined as Eq (07):

$$\tau'_{ij} = \rho \overline{u'_i u'_j} \quad \text{Eq (07)}$$

Where  $\overline{u'_i}$  and  $\overline{u'_j}$  are mean velocity fluctuation in  $x$  and  $y$  directions of Cartesian coordinates, respectively. If the density is constant the Reynold stress component can be represented as Eq (08):

$$\tau''_{ij} = \overline{u'_i u'_j} \quad \text{Eq (08)}$$

For three-dimensional space, six unique components of Reynold stress can be represented, where  $i$  and  $j$  can take values of  $x, y, z$  corresponding to Cartesian coordinates (Eq 09).

$$\begin{aligned} \tau''_{uu} &= \overline{u'^2} \\ \tau''_{vv} &= \overline{v'^2} \\ \tau''_{ww} &= \overline{w'^2} \\ \tau''_{uw} &= \overline{u'w'} \\ \tau''_{uv} &= \overline{u'v'} \\ \tau''_{wv} &= \overline{w'v'} \end{aligned} \quad \text{Eq (09)}$$

The Reynolds stress components play a key role in transporting momentum in turbulent flow, leading to the mixing and redistribution of fluid momentum. In this study, Reynold stress components of  $\overline{u'w'}$ , and  $\overline{w'v'}$  and  $\overline{w'^2}$  are used to characterize turbulent fluctuations in each canopy type. As the squared

horizontal turbulent velocity fluctuations (i.e.  $u'^2$  and  $v'^2$ ) can be prone to large errors in wave-affected environments (Hansen & Reidenbach, 2017), and the vertical velocity term  $w'$  has a less impact from waves due to elliptical structure of wave induced orbital velocities (Cannon et al., 2022), this term provides a more accurate representation of turbulent energy in the study conditions.

The Reynolds stress was employed for the estimation of boundary shear stress. There is no universally accepted methodology for calculating bed shear stress, particularly in complex, non-canonical boundary layers that exist within biological canopies, and various methodologies exist in the literature for its estimation (Yager et al., 2018).

In this study, the direct covariance measurement method was utilized to estimate boundary shear stress, as it has been observed to perform slightly better near the bed (Kim et al., 2000). and within complex flow fields such as oyster canopy (Kitsikoudis et al., 2020). The direct covariance measurement method estimates boundary shear stress based on the velocity time series variance and covariance, and it is also known as the Reynolds shear stress method. ( $\tau_{RS}$ , Eq 10). Here  $\rho$  is the density of water,  $\overline{u'w'}$  and  $\overline{v'w'}$  are Reynold stress components.

$$\tau_{RS} = \rho \sqrt{\overline{u'w'^2} + \overline{v'w'^2}} \quad \text{Eq (10)}$$

Friction velocity ( $u_*$ ) was estimated from the boundary shear stress to characterizes the effect of viscous shear stress at the solid boundary (Eq 11).

$$u_* = \sqrt{\frac{\tau_{RS}}{\rho}} \quad \text{Eq (11)}$$

The drag coefficient ( $C_d$ ) was determined by the ratio between the friction velocity ( $u_*$ ) and the horizontally- averaged velocity ( $U_0 = \sqrt{u^2 + v^2}$ , Eq 12, Schlichting, 2000; Whitman & Reidenbach, 2012)

to describe the resistance experienced by a fluid particle when moving through the flow field in the vicinity of a solid obstacle.

$$C_d = \frac{u_*^2}{U_0^2} \quad \text{Eq (12)}$$

Turbulent dissipation rate ( $\varepsilon$ ) was estimated using a second order structure function (Wiles et al., 2006), to represent the rate at which turbulent kinetic energy is being converted due to viscous dissipation of turbulent eddies. The second order structure function  $D(z, r)$  was defined at a location within the flow  $z$  using  $v'$  (fluctuation component of the velocity) (Eq 13).

$$D(z, r) = \overline{(v'(z) - v'(z + r))^2} \quad \text{Eq (13)}$$

$D(z, r)$  is the mean square of the velocity fluctuations difference between two points separated by distance  $r$ . The structure function was fit as shown in Eq 14:

$$D(z, r) = N + Ar^{2/3} \quad \text{Eq (14)}$$

where  $N$  account for Doppler noise and the coefficient  $A$  is defined as given Eq 15,

$$A = C_v^2 \varepsilon^{2/3} \quad \text{Eq (15)}$$

where  $C_v^2$  is an empirical coefficient with a value of 2 (Pope 2000) and  $\varepsilon$  is turbulent dissipation rate.

Turbulent production ( $P$ ) was calculated as the product of Reynolds stress and the velocity gradient ( $\frac{\partial \bar{u}}{\partial z}$  and  $\frac{\partial \bar{v}}{\partial z}$ , Tennekes & Lumley, 1972.) as shown in Eq 16:

$$P = \overline{u'w'} \frac{\partial \bar{u}}{\partial z} - \overline{v'w'} \frac{\partial \bar{v}}{\partial z} \quad \text{Eq (16)}$$

The turbulence intensity ( $u_{rms}$ ) was calculated as is the root mean square of the turbulent velocity fluctuation (Eq 17):

$$u' = u_{rms} = \sqrt{\frac{1}{N} \sum_i^N (u_i - \bar{u})^2} \quad \text{Eq (17)}$$

Scaled turbulence intensity is often used to explain the degree of turbulence present in a fluid relative to the flow velocity. The universal expression for turbulence intensity can be derived by normalizing raw intensity by the friction velocity (Eq 18-21).

$$\text{Intensity } x \text{ direction} = \frac{u'}{u^*} \times 100 \quad \text{Eq (18)}$$

$$\text{Intensity } z \text{ direction} = \frac{w'}{u^*} \times 100 \quad \text{Eq (19)}$$

$$\text{Intensity } y \text{ direction} = \frac{v'}{u^*} \times 100 \quad \text{Eq (20)}$$

$$y^+ = \frac{y}{h} \times 100 \quad \text{Eq (21)}$$

However, as friction velocity was originally defined for unobstructed flows, determining its value at oyster canopies poses challenges due to potential deviation from canonical boundary layer scaling. Turbulence within these canopies is generated from the combination of bed shear stress and oyster canopy interaction (Cannon et al., 2022). Given the uncertainty of estimating friction velocity complex flows such as found within oyster canopy (Kastner-Klein & Rotach, 2004) normalization was done using a turbulent velocity scale derived from locally measured Reynolds shear stress. This approach has been adopted by researchers in similar environments (D. Cannon et al., 2022; Reidenbach et al., 2006). Researchers such as Nakagawa et al., (1975) and Nezu, (1977) among others, have described turbulence intensity variation with channel depth ratios ( $y/h$ ) over rough beds, where  $y$  is the distance from the bed to the flow measuring point and  $h$  is the water depth. This enables the comparison of turbulence in the main sub-regions of the channel, such as the wall region, intermediate region, and free stream region. In this study, turbulence intensity is compared in regions of flow within the oyster canopy and directly above the oyster canopy.

### **Quadrant Analysis**

Quadrant analysis (Lu & Willmarth,1973) was undertaken to describe how instantaneous turbulent fluctuations contribute to momentum distribution throughout the boundary layer of each canopy type. A quadrant analysis was conducted, separating the  $u'$  and  $w'$  velocity component from the canopy flow velocity data into four quadrants based on the sign of their instantaneous values. Here  $u'$  and  $w'$  are calculated by subtracting the mean flow,  $\bar{u}$  from the instantaneous velocity,  $u_i$ .

After computing the values of turbulent velocity fluctuations ( $u'$  and  $w'$ ), a probability distribution function (PDF) for the Reynolds stress associated with the product  $u'w'$  was determined. This PDF was then utilized to generate contour plots, enabling the identification of Reynolds stress distribution across quadrants. These plots were analyzed as visual aids to understand the spatial distribution of Reynolds stress concerning flow ejections and sweeping motions.

## CHAPTER FOUR: RESULTS

The results can be categorized into two main sections according to scale. Reef-scale results document the influence of the reef as a whole on local flow patterns, whereas canopy-scale results document the variability within the reef. At the reef scale, the study hypothesizes that the reef will attenuate incident hydrodynamic energy and that the reef's effect to the local flow field will vary with water level. Canopy-scale results test the hypothesis that flow hydrodynamics will be influenced and altered by the various canopy density types present within the oyster reef ecosystem. Since the data collection was conducted in a highly dynamic environment where external factors, such as water level, wind, and flow speed, vary temporally, reef-scale results explain the interaction of ambient environmental factors with the reef, supporting a clearer understanding of the canopy-scale results. Despite the experiment being conducted under varying water levels, including high and low water conditions, it's notable that the H-DEN canopy remained unsubmerged during low water levels. Consequently, data collection was not possible for either within- or above-canopy measurements for the H-DEN canopy during these low water periods.

### Reef-scale Hydrodynamics

Ambient environmental conditions (wind speed and direction, water level and current speed) varied from the Spring (seasonal low water level measurements) to Fall (seasonal high water level measurements). Throughout data collection, the prevailing wind direction was from northeast to southwest. Median wind speeds during low water level measurements varied within the range of 2.5 to 3.2 m/s, and were only slightly greater during high water levels, varying within the range of 2.5 to 4.8 m/s (Fig. 6a& b). Within seasons, wind conditions recorded from day to day varied only slightly (Table 1). For instance, during the high water level measurements, windspeeds recorded on the day that the H-DEN canopy flows were measured were 0.8-4.6 m/s, almost 48% lower than the day the SPA canopy flows were measured.

Table 1. Relative wind speed and direction recorded with respect to SPA high and low water.

Water Level	Canopy	Speed (%)	Direction (degrees)
Low	MOD	-14.4	81.7
Low	DEN	-28.8	26.9
High	MOD	-22.1	52.4
High	DEN	-7	63.2
High	H-DEN	-48	3.6

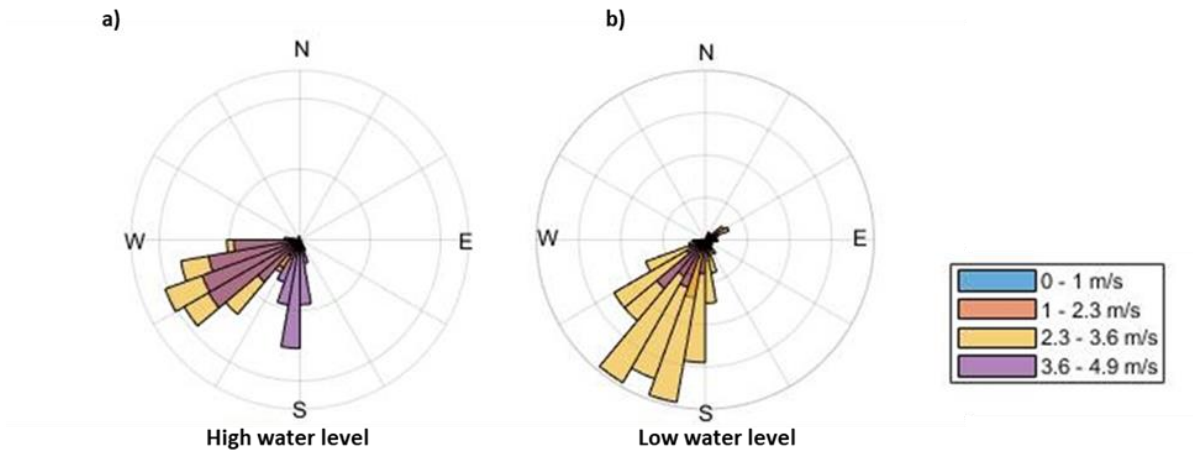


Figure 6. Wind speed and direction recorded during seasonal a) high and b) low water levels.

The water level in the channel and over the reef increased consistently throughout the flood tide data collection period each day (Fig. 7). The change in tidal amplitude varied throughout the study period, with amplitude ranging from 3 to 22 cm during high water level measurements and remaining consistent (~7 cm) throughout all low water level measurement days.

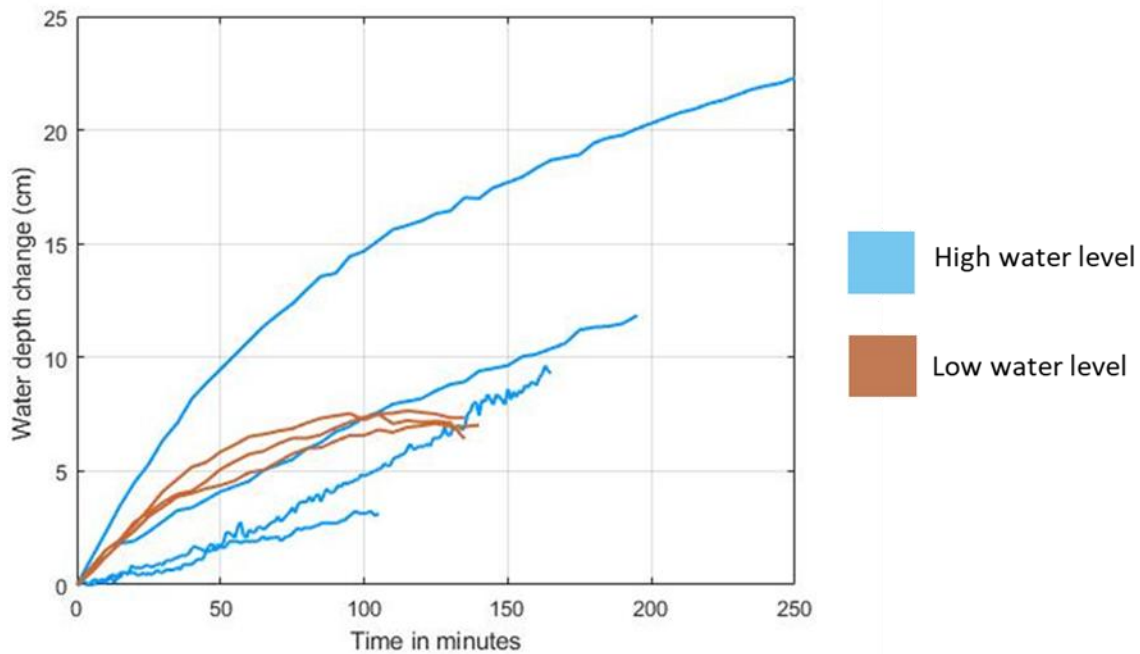


Figure 7. Channel depth variation during high (H) and low (L) water level measurements.

### Current Direction and Magnitude

Analysis of current direction in the channel, incident to the reef and above/within the reef canopy indicates that flow-reef interaction was governed primarily by water level with respect to the reef crest. During the seasonal low-water condition, the reef was not fully submerged even at high tide, whereas the reef was fully submerged for much of the time during the seasonal high-water condition. When the reef crest was exposed, tidal currents were routed around the reef, producing flow directionality above and within the reef canopy that sometimes varied substantially from the channel and incident flow direction (Fig. 8a, Table 2). However, when the reef crest was fully submerged and water flowed over the reef, current directions above the reef canopy were better aligned with the incoming flow (Fig. 8b). Flow direction within the canopy was generally dispersed over a wider range than above-canopy flows, suggesting the influence of flow interaction with canopy elements.

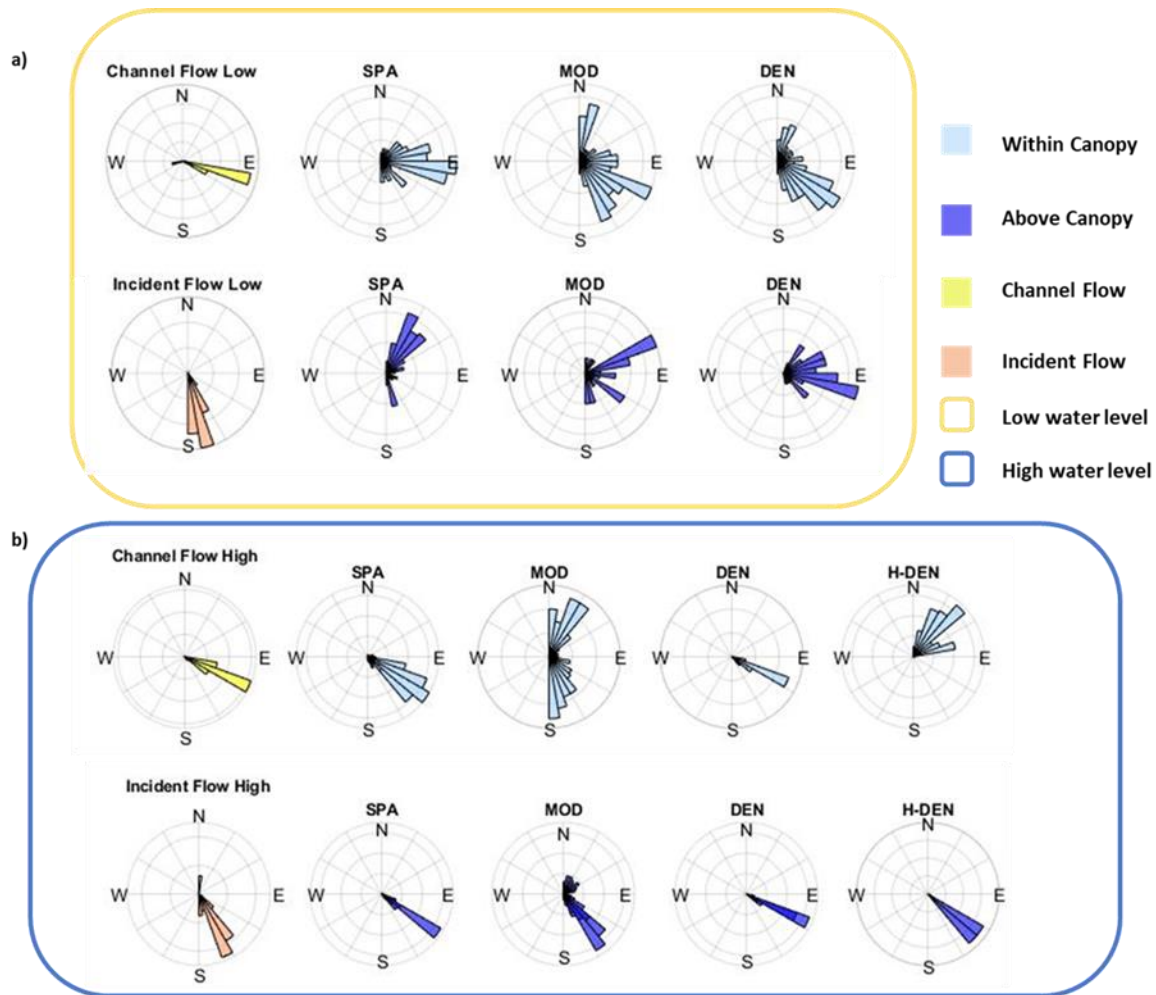


Figure 8. Stream flow directionality within and above the canopy at: a) low water level, b) high water levels.

During low water measurements, mean flow speeds within the canopy were very low ( $< 1$  cm/s) and gradually decreased as canopy density increased (Fig. 9a). Above the canopy, velocities were also typically below 2 cm/s during the low water measurements. Within-canopy flow speeds increased marginally during high-water measurements, with the highest mean within-canopy flow recorded in the DEN canopy (2.4 cm/s). However, flow speeds increased more substantially above the canopy, where the highest mean stream flow was recorded above the H-DEN canopy (10.29 cm/s, Fig. 9d, Table 2).

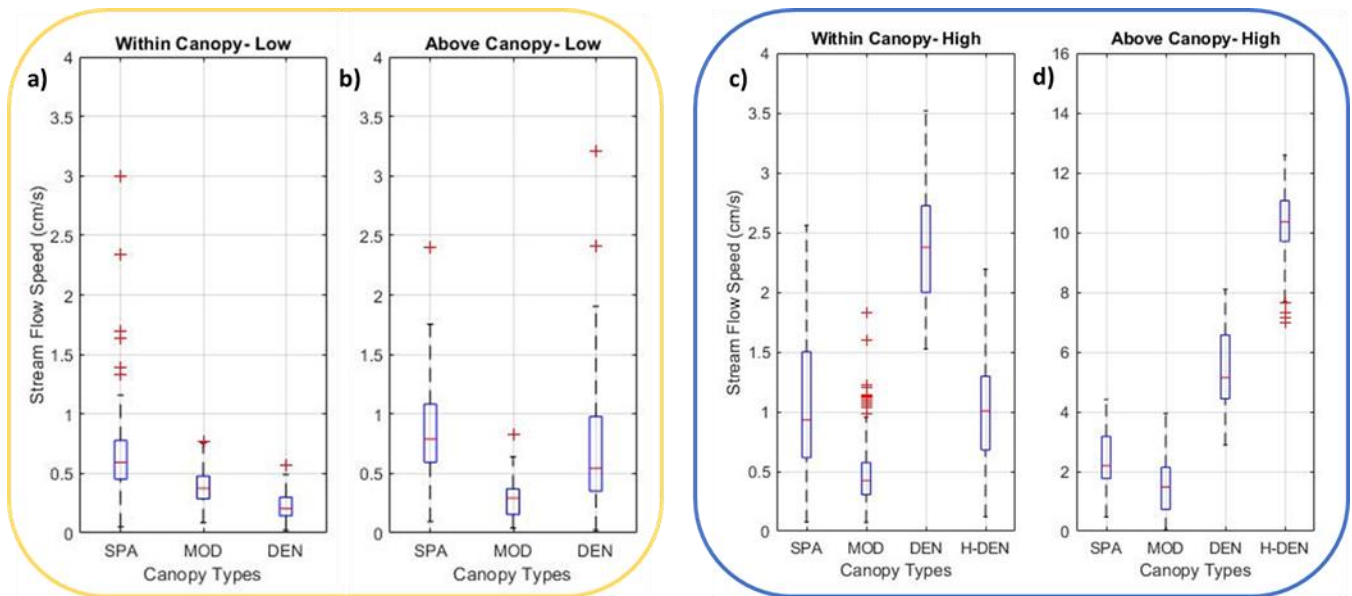


Figure 9. Boxplots of current speed observed during at low water levels a) within and b) above the canopy, and at high water levels c) within and d) above the canopy. Note the different y-axis scaling in part d.

Moreover, overall flow statistics can be derived for each location considering both low and high water levels. It can be said that the incident flow gradually diminishes as it progresses: first from above the canopy, and then is at a minimum within the canopy itself (Fig. 10). The one exception to this pattern is observed at the H-DEN above the canopy, where flow is higher than the incident flow. This exception can be attributed mainly to the development of a shear layer above the canopy of H-DEN due to its dense and uniform canopy structure.

Table 2. Within- and above-canopy flow statistics with flow direction change shown relative to the channel flow direction.

Water Level	Location	Direction change (degrees)	Direction	Speed (cm/s)		
				Min	Mean	Max
<b>Within Canopy</b>						
Low	SPA	25	East	0.05	0.68	2.99
	MOD	264	East to South	0.09	0.39	0.77
	DEN	24	East to South	0.02	0.23	0.57
High	SPA	12	East to South	0.08	1.07	2.56
	MOD	316	North to South	0.07	0.48	1.83
	DEN	10	East to South	1.52	2.39	3.52
	H-DEN	120	North to East	0.12	1.00	2.19
<b>Above Canopy</b>						
Low	SPA	287	North to East	0.10	0.81	2.40
	MOD	43	North to East	0.04	0.30	0.82
	DEN	4	East	0.02	0.76	3.21
High	SPA	13	East to South	0.48	2.40	4.41
	MOD	18	East to South	0.04	1.52	3.94
	DEN	9	East to South	2.88	5.35	8.09
	H-DEN	157	East to South	6.97	10.29	12.59

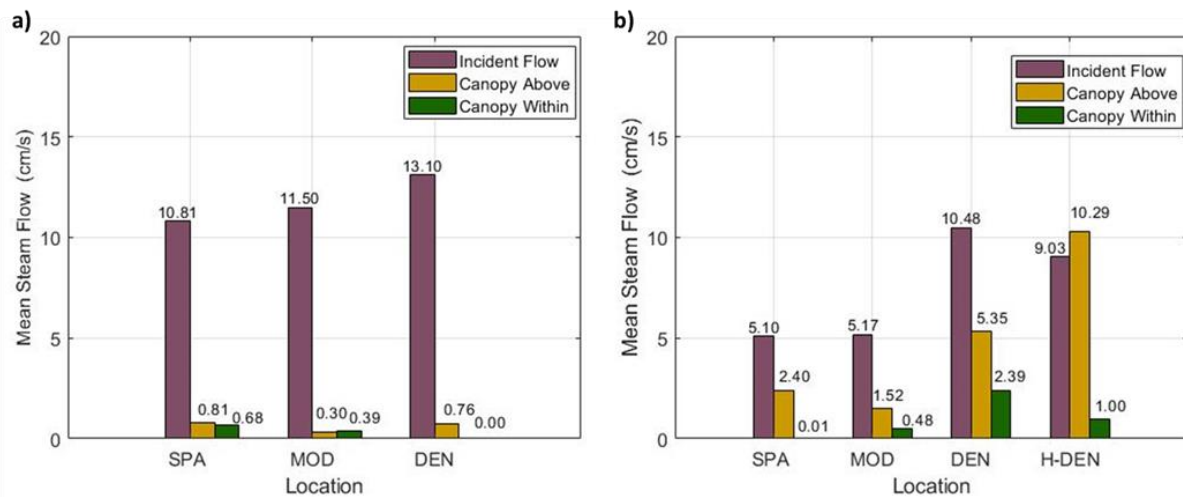


Figure 10. Mean flows incident to the reef and above and within the canopy during a) low water levels and b) high water levels.

## Canopy-scale Hydrodynamics

This section examines hydrodynamic variation in the oyster canopy and distinguishes hydrodynamic parameters among different canopy types and positions with respect to the canopy. It commences by presenting the findings derived from velocity attenuation rates specific to each canopy type. Following this, turbulence intensity and its distribution are presented. Furthermore, a comprehensive analysis of turbulence generated by the canopy is conducted, focusing on parameters such as turbulence dissipation and production. Additionally, canopy drag coefficients specific to each canopy type are estimated. Finally, insights into the structure of turbulence stemming from the canopy is presented, employing contour plots for visualization.

### Velocity Attenuation

Velocity attenuation is assessed in the context of channel flow and incident flow near the reef. Analyzing velocity attenuation enables understanding the extent to which the reef and canopy impact the flow. Velocity attenuation at low water levels within and above the canopy was uniformly high with respect to incident flows (Fig. 11a-b); attenuation values almost always surpassed 90%, with similar values across canopy types. All canopies typically exhibited slightly higher attenuation in incident flow than in channel flow, reflecting that flows generally were attenuated slightly along the channel slope approaching the reef (Fig. 12a-b). When water levels were high, attenuation rates varied among the canopy types and more variation with respect to canopy position was evident.

Within the canopy, MOD, DEN, and H-DEN all attenuated more than 90% of the incident flow, while lower attenuation of approximately 70% was observed within the SPA canopy. By comparison, above-canopy attenuation was lower, at around 48% for the SPA canopy and 64-65% for the MOD and DEN canopies. Interestingly, above the H-DEN canopy, attenuation was negative, indicating that the flow speed above this

canopy was higher than incident flow- near the reef. This indicates formation of a shear layer over the canopy due to its homogeneous canopy structure arrangement (Fig. 12c&d).

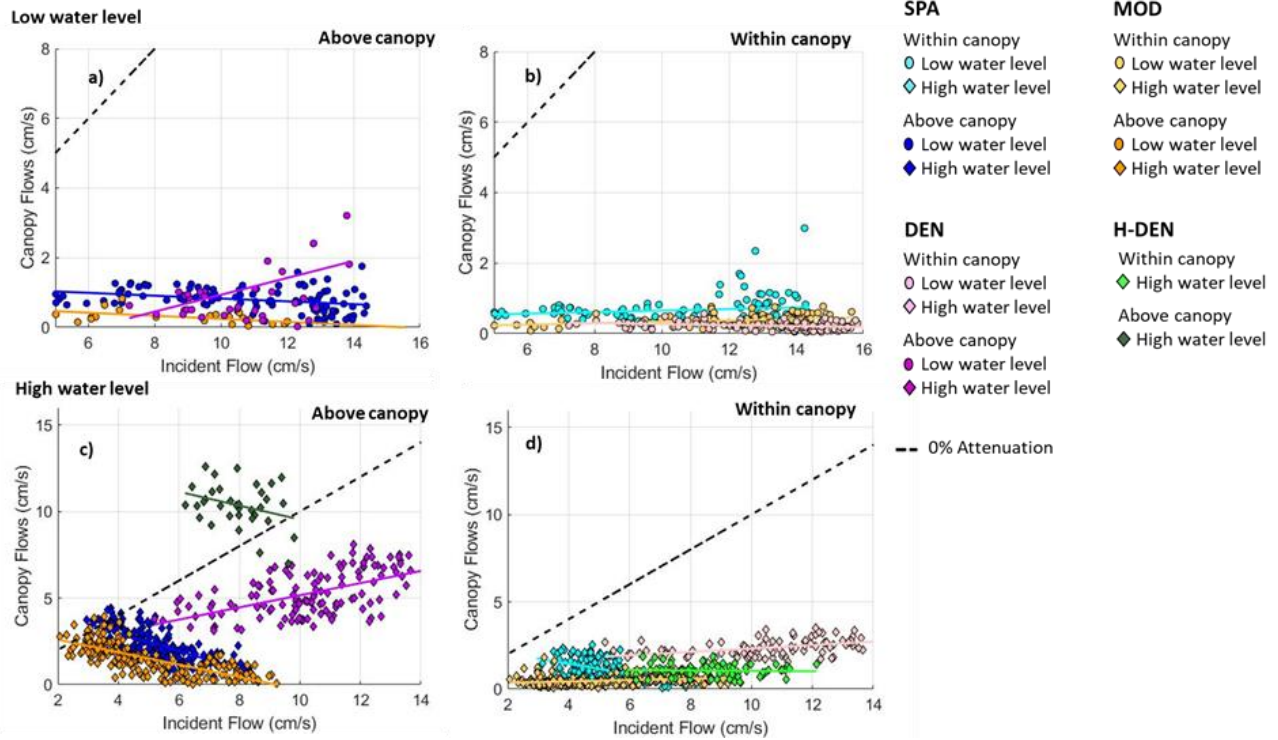


Figure 11. Velocity attenuation from incident to canopy flows by canopy density during low water levels a) above and b) within the canopy, and during high water levels c) above and d) within the canopy. The black dashed 1:1 line represents no change in velocity.

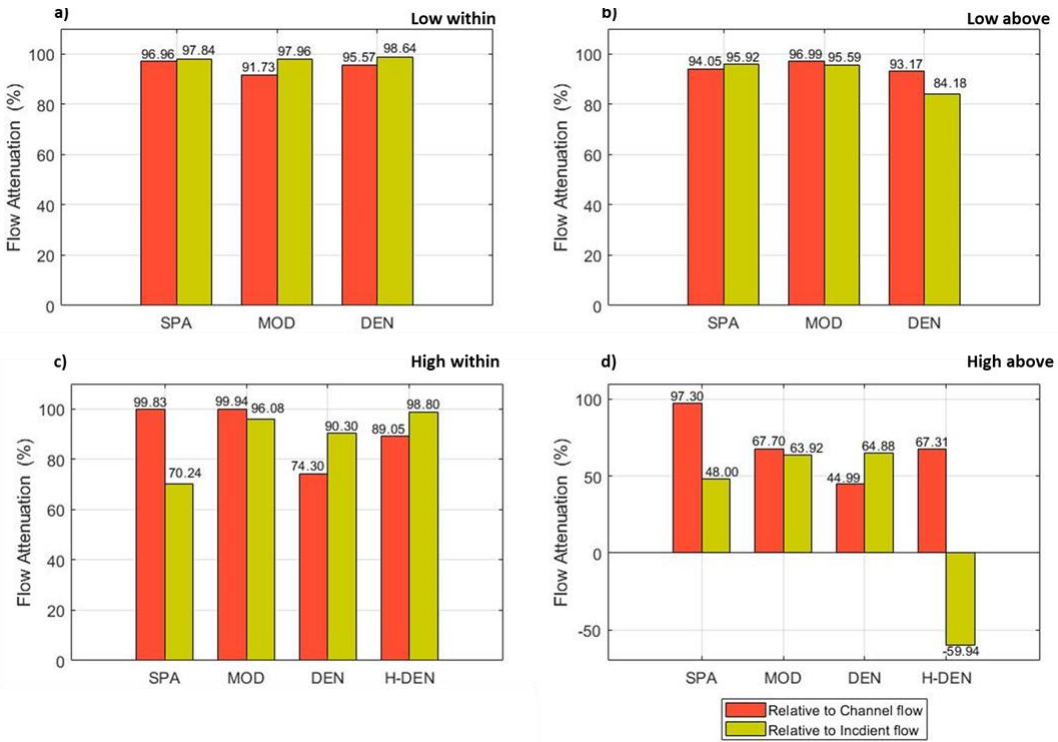


Figure 12. Mean velocity attenuation relative to channel and incident flows during low water levels a) within and b) above the canopy, and during high water levels c) within and d) above the canopy.

### Turbulence Production and Dissipation

Turbulence dynamics can be quantified and analyzed into dissipation and production terms based on the turbulence budget equation, focusing on how these components vary across the canopy (Fig. 13). During periods of low water levels, the water column was insufficient to calculate turbulence parameters above the canopy. Additionally, the H-DEN canopy remained unsubmerged; hence, neither within-canopy nor above-canopy data was collected for the H-DEN canopy during low water levels.

Within the SPA canopy, turbulence production dominated during periods of low water levels, though both production and dissipation were consistently low over the data collection period. Notably, dissipation remained relatively constant, whereas production exhibited numerous fluctuations (Fig.13b). Conversely, during periods of high-water levels within the SPA canopy, production consistently dominated, especially

towards the end of the flood tide when fluctuations were more pronounced. Above the canopy, dissipation prevailed consistently throughout the observation period, with the amplitude of turbulent production decreasing towards the end of the flood tide (Fig. 13a).

In the MOD canopy, dissipation was dominant during low water levels and began to decrease as water depth incrementally increased. Both turbulence production and dissipation displayed higher fluctuations during this period (Fig. 13d). Similarly, during high water levels within the MOD canopy, dissipation remained dominant and consistent, while production exhibited higher levels of fluctuation, especially during a slow increase in water depth. Above the canopy, production dominated, with higher fluctuations observed compared to dissipation, indicating a more intense injection of energy into the system (Fig. 13c).

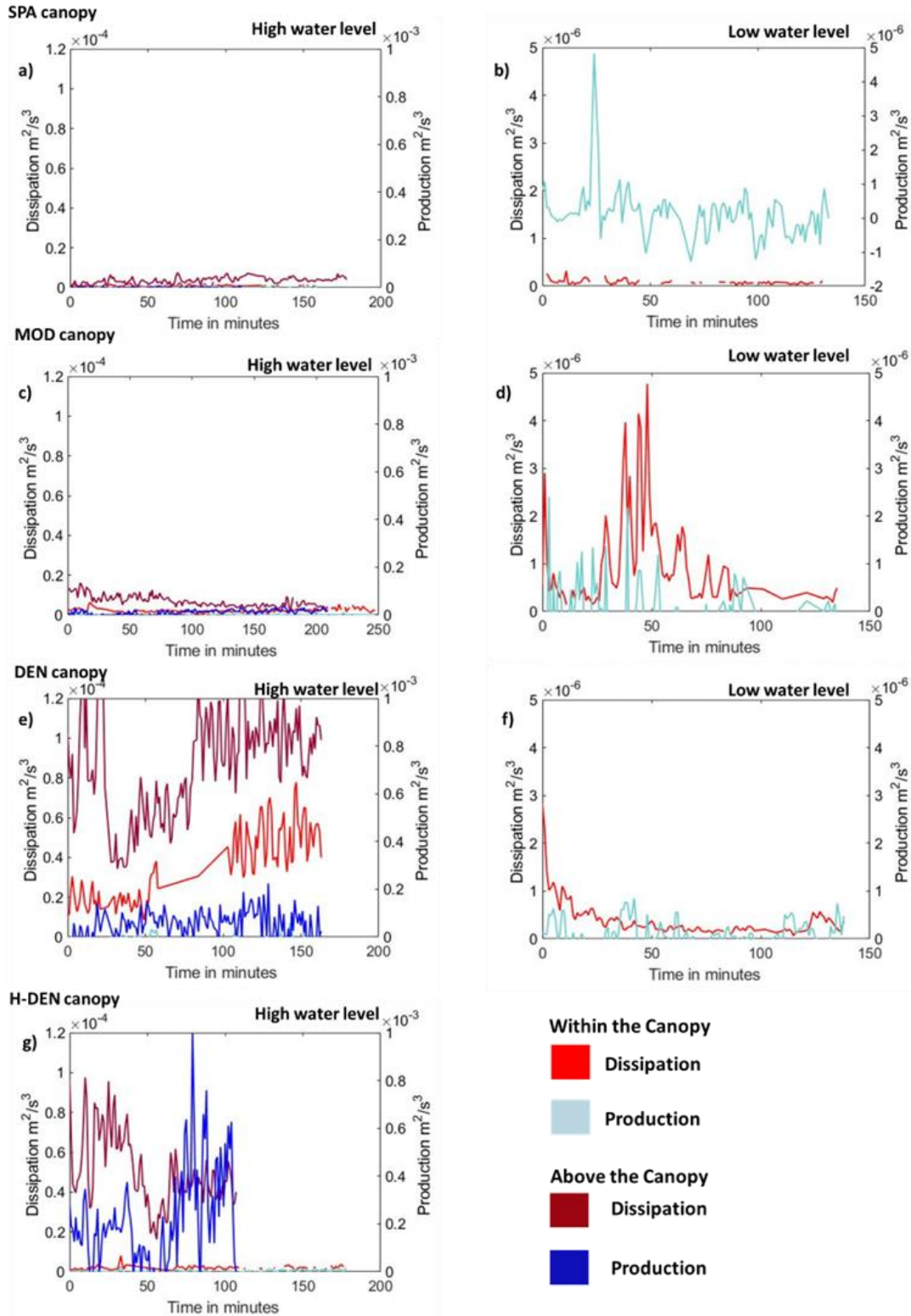


Figure 13. Turbulence dissipation and production time series within and above the canopy during high and low water levels: a-b) SPA, c-d) MOD, e-f) DEN, g) H-DEN.

Within the DEN canopy, dissipation dominated during periods of low water levels and remained consistent throughout the data collection period. Turbulence production exhibited higher fluctuations (Fig. 13f). During high water levels within the DEN canopy, turbulence dissipation remained dominant, aligning closely with the increasing water depth trend. Production remained relatively consistent throughout this period. Above the canopy, dissipation prevailed over production, gradually increasing over the data collection period. Turbulent production displayed higher fluctuations, suggesting an intensified energy injection (Fig. 13e).

In the HDEN canopy, turbulence production dominated within the canopy, characterized by numerous fluctuations, while dissipation remained relatively consistent but lower than production values. Above the canopy, turbulent production was observed at a high level, accompanied by pronounced bursting phenomena. Additionally, during the middle of the data collection period, a reduction in the rate of change in water depth led to an increase in production. Turbulence dissipation-maintained consistency, similar to within the canopy (Fig. 13g).

Upon calculation and plotting of the mean turbulence dissipation and production parameters for each canopy type, it was observed that the average values of turbulence production and dissipation recorded during low water levels ranged approximately from  $(0.09 - 0.94) \times 10^{-6} m^2 s^{-3}$  and  $(0.27 - 0.59) \times 10^{-6} m^2 s^{-3}$  respectively (Fig 19a). Similarly, for the high-water level, there were notably higher turbulence production and dissipation values, approximately two orders of magnitude higher for both within and above the canopy. Within the canopy, the average values ranged from  $(0.01 - 0.35) \times 10^{-4} m^2 s^{-3}$  and  $(0.02 - 0.14) \times 10^{-4} m^2 s^{-3}$  for turbulence dissipation and production respectively. Above the canopy, turbulence production and dissipation levels ranged from  $(0.04 - 0.87) \times 10^{-4} m^2 s^{-3}$  and  $(0.02 - 2.61) \times 10^{-4} m^2 s^{-3}$  respectively (Fig. 13a, c & g, Fig. 14c&e).

When conducting further analysis of the canopy, types, it was observed that for the SPA the highest mean turbulent parameters were found to be  $0.03 \times 10^{-4} \text{ m}^2\text{s}^{-3}$  (within the canopy high water level) and  $0.04 \times 10^{-4} \text{ m}^2\text{s}^{-3}$  (above the canopy high water level) for turbulent production and dissipation respectively. For the MOD Canopy, the highest mean turbulent parameters were  $0.02 \times 10^{-4} \text{ m}^2\text{s}^{-3}$  (within the canopy high water level) and  $0.07 \times 10^{-4} \text{ m}^2\text{s}^{-3}$  (above the canopy high water level) for turbulent production and dissipation respectively. Similarly, for the DEN Canopy, the highest mean turbulent parameters were  $0.71 \times 10^{-4} \text{ m}^2\text{s}^{-3}$  (above the canopy high water level) and  $0.87 \times 10^{-4} \text{ m}^2\text{s}^{-3}$  (above the canopy high water level) for turbulent production and dissipation respectively. Lastly, for the H-DEN Canopy, the highest mean turbulent parameters observed were  $2.61 \times 10^{-4} \text{ m}^2\text{s}^{-3}$  (above the canopy high water level) and  $0.5 \times 10^{-4} \text{ m}^2\text{s}^{-3}$  (above the canopy high water level) for turbulent production and dissipation respectively.

Since these values were collected on different days, direct comparison of dissipation and production values among canopy types is challenging. However, by plotting the ratio of turbulence production to dissipation, it is still possible to analyze which turbulent parameter dominates among the canopy types, even without normalization.

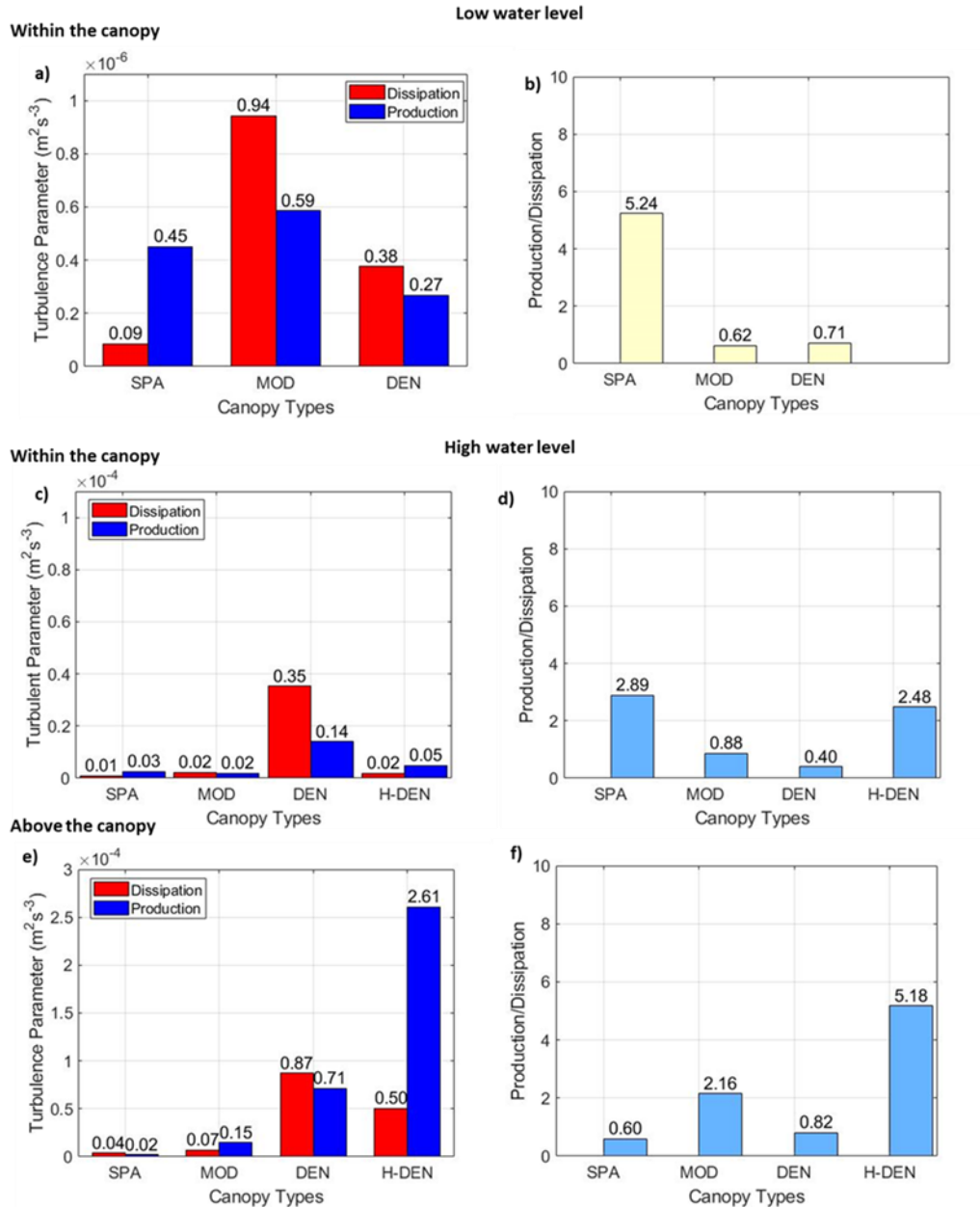


Figure 14. Mean turbulence production and dissipation (a, c & e) and ratios of production to dissipation (b, d & f).

When observing the turbulence production to dissipation ratios in low water levels within the canopy, except for SPA canopies, turbulence dissipation is dominant in the rest of the canopies (Fig. 14b). Moreover, a higher ratio between production and dissipation is observed in the SPA canopy. For high water levels, it is observed that within the canopy, SPA and HDEN canopy types have turbulence production

dominance, while MOD and DEN canopies have dissipation dominance (Fig. 14d). Above the canopy, MOD and HDEN have turbulence production dominance, while SPA and DEN canopies have turbulence dissipation dominance (Fig. 14f). This insight helps to quantify the differences among canopy types more clearly in terms of turbulence.

Comparing turbulence production and dissipation within and above different canopy types reveals notable variations. Within the SPA canopy during high water levels, turbulence production within the canopy was approximately 0.6 times smaller, while dissipation was roughly 4 times larger. In contrast, within the MOD canopy, mean production above the canopy was approximately 8 times larger, while dissipation was roughly 4 times larger than within the canopy. Similarly, within the DEN canopy, the mean production above the canopy is expected to be approximately 5 times larger, while dissipation is projected to be about 2.5 times larger. However, when comparing turbulence production and dissipation between above and within the HDEN canopy, the ratio indicates a substantial difference. Above the canopy, mean turbulent production is projected to be approximately 52 times larger, while dissipation is estimated to be about 25 times larger. (Fig. 14c&e)

### **Turbulence Intensity**

When plotting the turbulent intensity values relevant to each canopy type against the depth ratio on the same platform, it is evident that except for HDEN above, the rest of the canopy types exhibit a relatively similar distribution (Fig. 15). However, a key distinction lies in the fact that the HDEN canopy exhibits slightly higher turbulence intensity variation values, spanning an intensity ratio range between 2 and 7. In contrast, the turbulence intensity values for the other canopies are distributed within the range of 1 to 5. Additionally, it is noteworthy that only MOD, DEN, and H-DEN canopies show turbulence values beyond the depth ratio of 0.2, extending beyond the wall region.

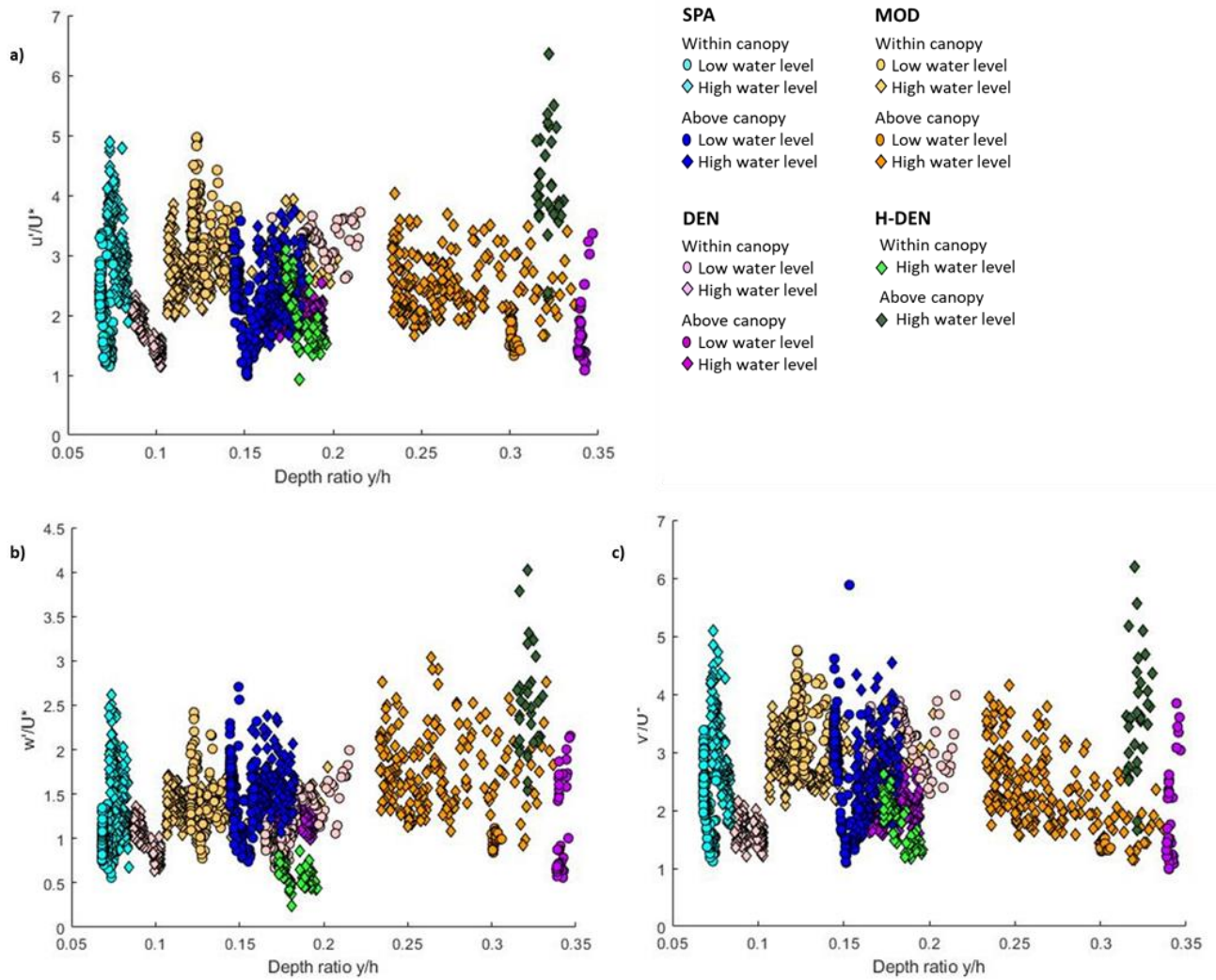


Figure 15. Turbulence intensity in all the canopies based on water levels: a) Considering full depth profile stream flow direction, b) Vertical direction c) Cross channel direction.

Notable variation of turbulence intensity values unique to each canopy type was observed when calculating the mean intensity values for each canopy type (Fig. 16). When observing the mean turbulence intensity values at high and low water levels, notable differences can be seen, especially in canopies such as DEN and MOD. This discrepancy is mainly influenced by the varying water levels received at the study site during high and low water levels, affecting the fluctuation behavior of turbulence. Hence, it is suitable to analyze the turbulence intensity values separately for high and low water levels.

During high water levels, the highest intensities are recorded above the canopy of HDEN, more than two times higher than the intensities observed within the HDEN canopy. In the DEN canopy, intensities above the canopy are slightly higher than within, while in the MOD canopy, intensities within the canopy are slightly higher than above. Interestingly, in the SPA canopy, both above and within the canopy exhibit similar and balanced turbulence intensity values, a phenomenon also observed at low water levels.

In low water levels, the highest intensities are observed within the canopy of MOD and DEN, with intensity values higher than those during high water levels. This is likely due to flow restrictions and flow recirculation. The reduced water volume during low water levels may cause the space between canopy elements to decrease, leading to increased flow restriction and intensified turbulence within the canopy as the flow navigates through narrower gaps.

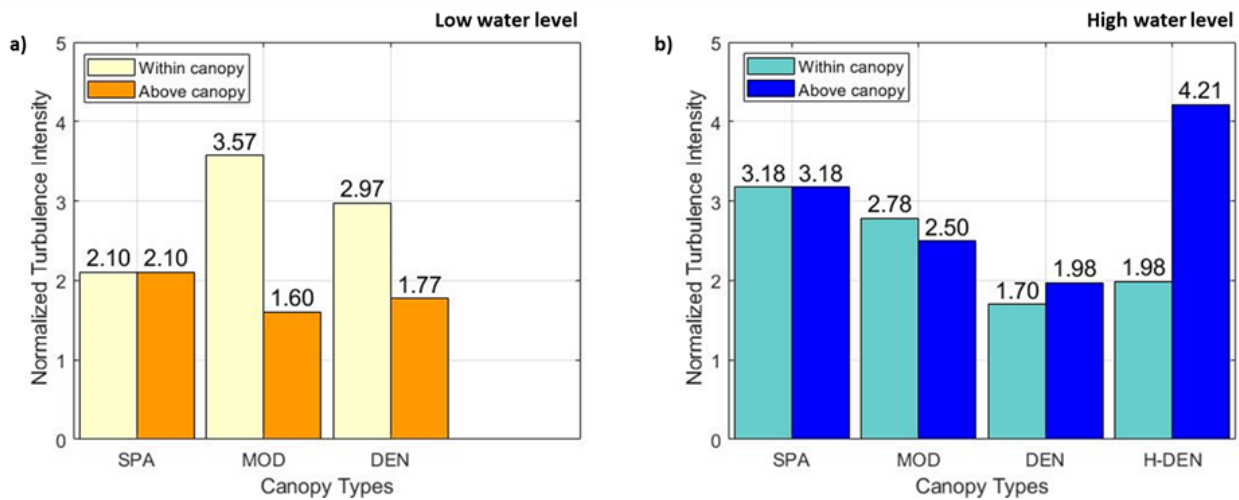


Figure 16. Mean normalized turbulence intensities across different canopy densities: a) Low water level, b) High water level.

Similarly, when observing the behavior of turbulence intensity in the cross-channel and vertical directions, a consistent pattern of intensity distribution along the channel emerges. However, in the vertical direction ( $w'$ ), turbulence intensity values are slightly lower compared to those in the along-channel and cross-channel directions (Fig. 15b&c).

## **Drag Coefficient**

When analyzing the drag coefficients during the high water level experimental data collection period, notable variability was observed, highlighting the dynamic nature of the study area (Fig. 17). Notably, both within and above the canopy, frequent fluctuations with substantial amplitudes were observed. The drag coefficient remained relatively stable in most of the canopy types, except above the MOD canopy, where it started to decrease towards the end of the flood tide (end of data collection, Fig. 17d). Conversely, in the H Den above the canopy, the drag coefficient exhibited an increase towards the end of the flood tide (Fig. 17h). Mean drag coefficients were computed from the time series data to delineate the canopy-specific effects. The low water level drag coefficients were not considered due to the low flow velocities observed in the study area.

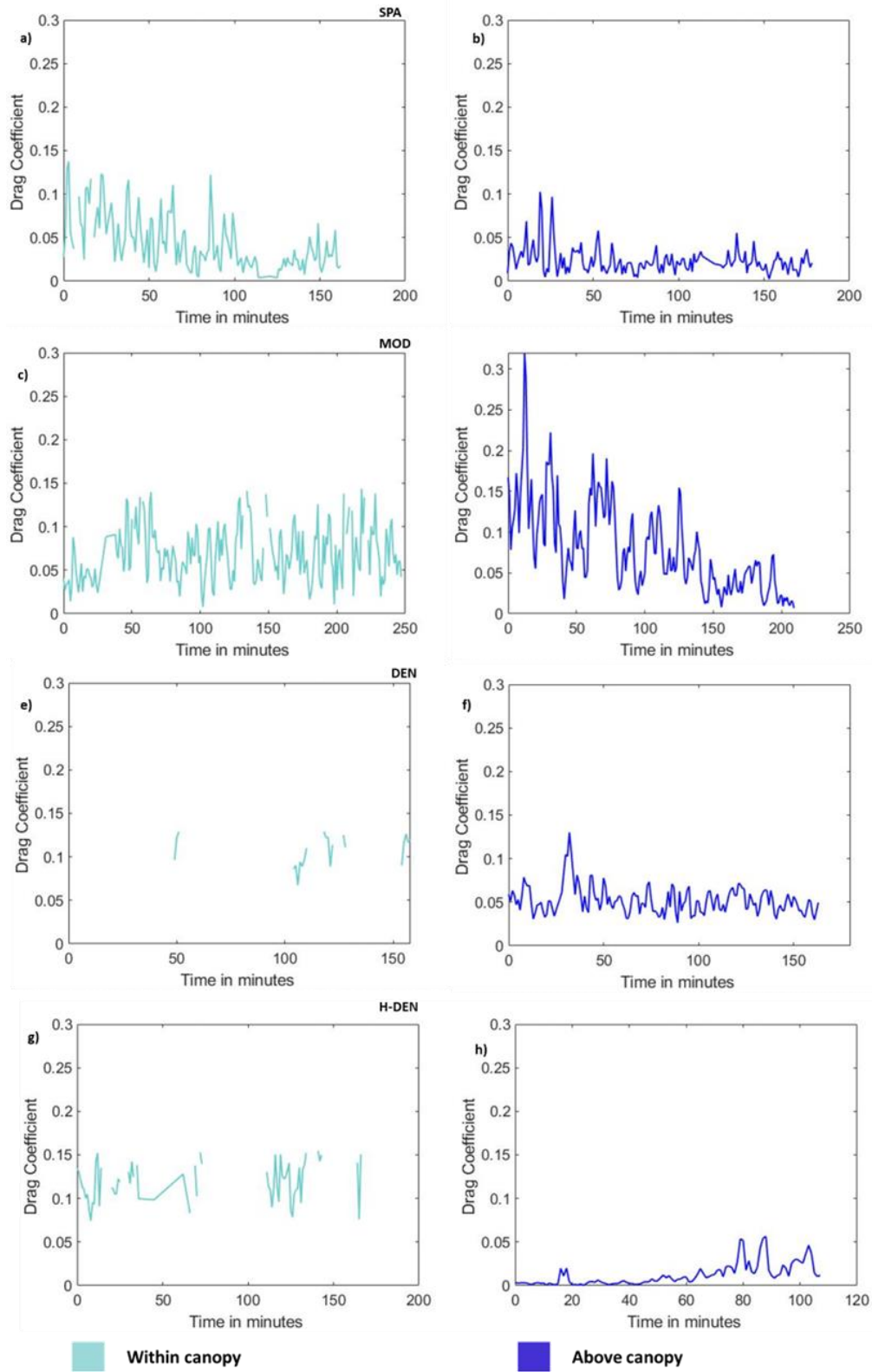


Figure 17. Variability of drag coefficients observed during high water level above and within canopies of varying density: a-b) SPA canopy, c-d) MOD canopy, e-f) DEN canopy, g-h) H-DEN canopy.

Mean drag coefficients recorded within the canopy ranged from 0.04-0.12 and tended to increase with canopy density (Fig. 18a). Within-canopy drag coefficients were generally larger than those observed simultaneously above the canopy (0.01-0.08, Fig. 18a-b). The exception was observed in the MOD canopy, where the mean above-canopy drag coefficient was slightly larger than within the canopy (0.08 above canopy as compared to 0.07 within canopy). Drag coefficients observed above the H-DEN canopy were the lowest observed and the ratio of within and above-canopy drag coefficients was approximately five times larger than the other canopy types, reflecting the production of the shear layer above the H-DEN canopy (Fig. 18b).

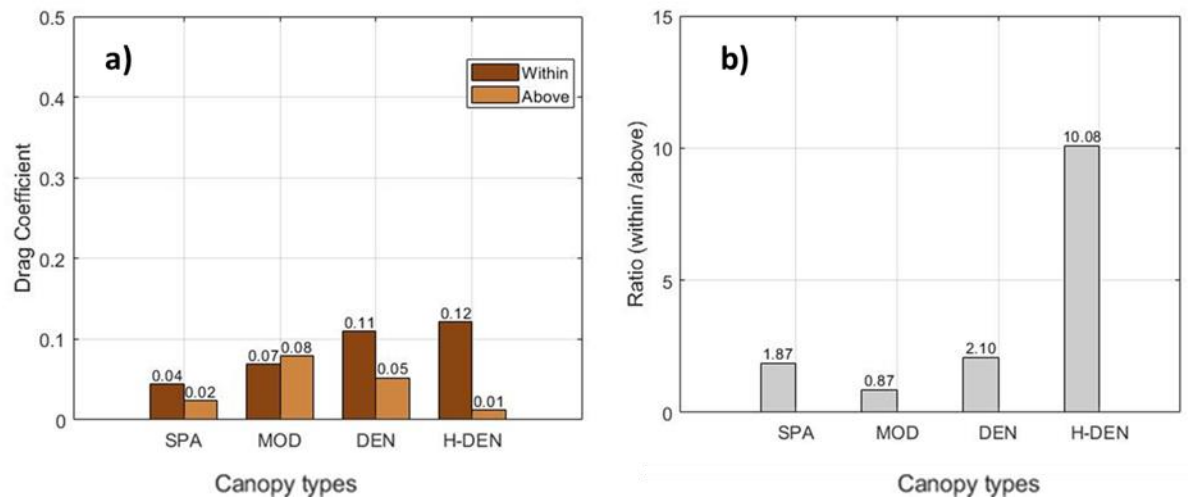


Figure 18. Comparison across canopy density of a) mean drag coefficients within and above canopy and b) ratio between within- and above-canopy mean drag coefficients.

### Quadrant Analysis

In interpreting the quadrant analysis within the study coordinate system, positive values of  $w'$  indicate upward turbulence intensity, suggestive of turbulent ejection motions, while negative values imply downward motion toward the bed, indicative of sweeping motion. Similarly, positive  $u'$  and negative  $u'$  suggest intensities moving in the west and east directions, respectively. Within the SPA canopy during

low water levels, it was observed that Q1 and Q4 exhibit higher stress values. It can be inferred that Q1 slightly dominates in this scenario. Above the canopy, the majority of intensities are distributed in Q1 and Q4 quadrants, with Q4 dominating (Fig. 19a-b). During high water levels, directionality within the canopy is opposite to that of low water levels. Q3 and Q2 have the highest distribution, and Q3 dominates. Similarly, the majority of intensities above the canopy are distributed in Q2 and Q3 quadrants. However, here, Q3 slightly dominates (Fig. 19c-d). Also, it is observed that the quadrants Q1 and Q3 are linked together in all scenarios.

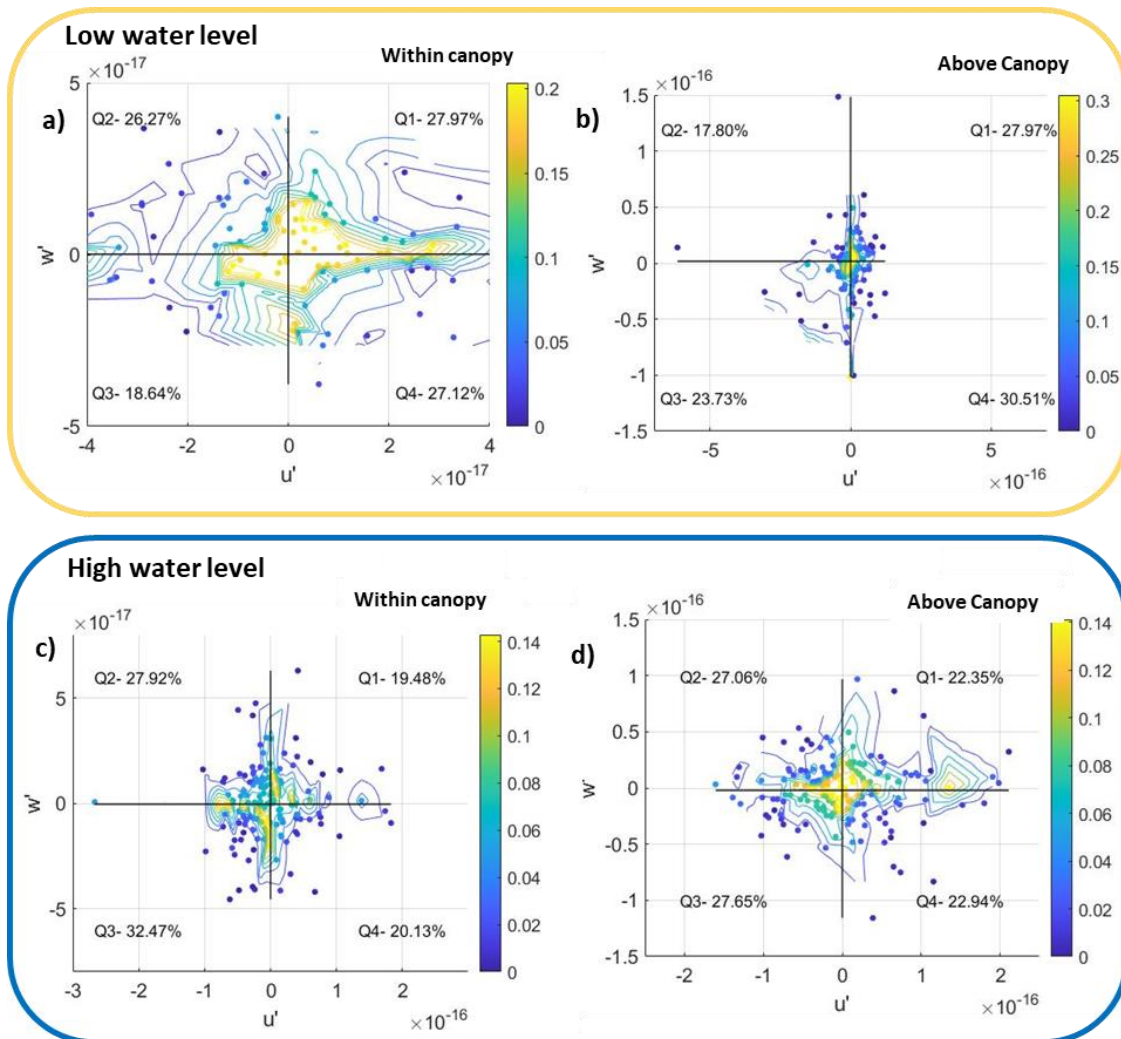


Figure 19. Quadrant analysis for SPA canopy observed during low water levels a) within and b) Low above the canopy and during high water levels c) within and d) above the canopy.

Within the MOD canopy during low water levels, it is observed that Q3 and Q4 exhibit higher stress values. It can be inferred that Q4 slightly dominates in this scenario. Above the canopy, intensities are distributed among the Q2 and Q3 quadrants, with Q4 dominating (Fig. 20a-b). During high water levels within the MOD canopy, Q1 and Q4 have the highest distribution, with Q4 dominating. Similar to high within the canopy, the majority of intensities are distributed equally in Q1 and Q2, and Q4 quadrants above the canopy. However, here, Q4 is slightly dominating (Fig. 20c-d). Additionally, it is observed that the quadrants Q1 and Q3 are linked together during both high and low water levels.

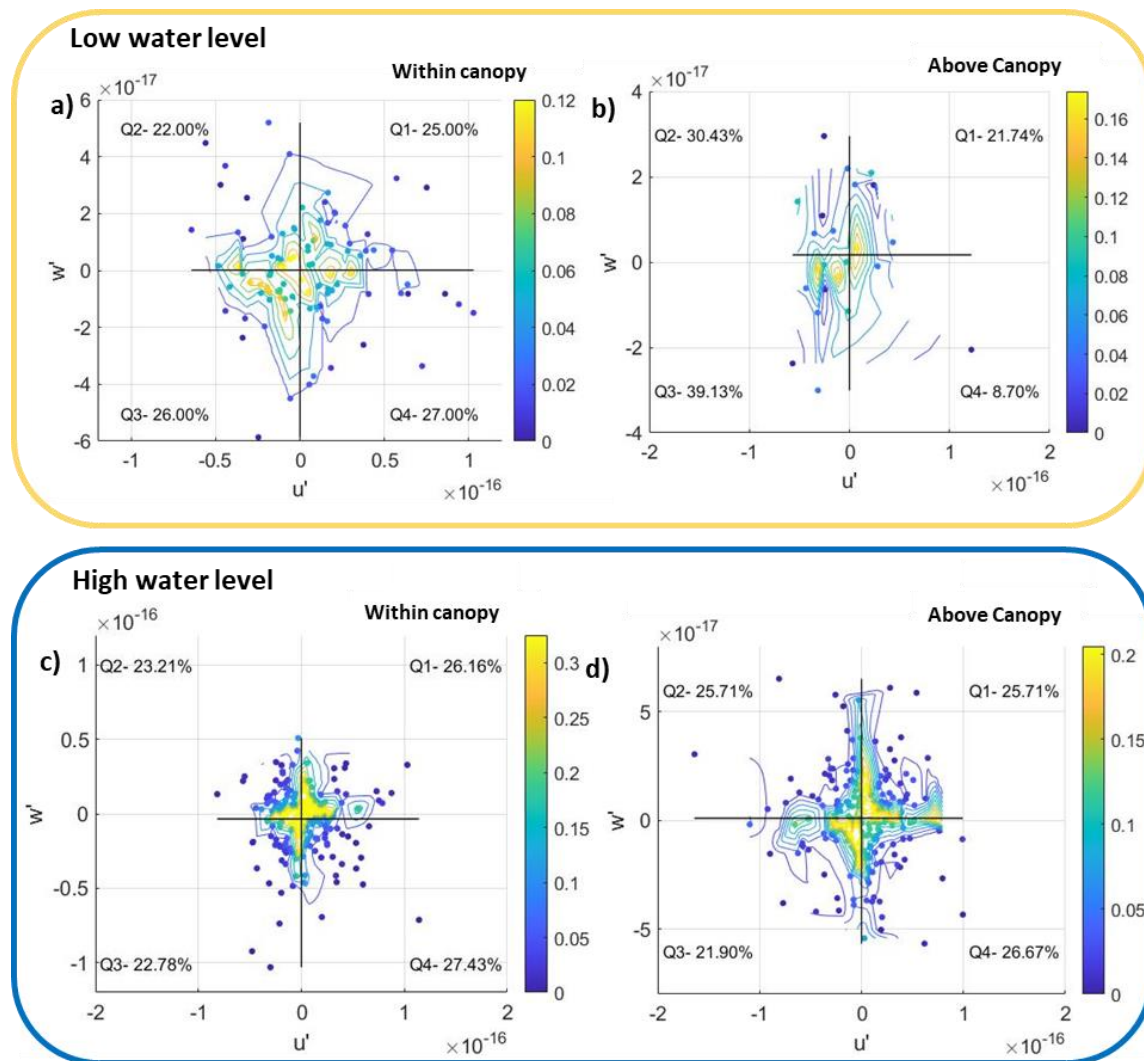


Figure 20. Quadrant analysis for MOD canopy observed during low water levels a) within and b) above the canopy and during high water levels c) within and d) above the canopy.

Within the DEN canopy during low water levels, Q3 and Q4 exhibit higher stress values, with Q3 slightly dominating the overall distribution. In the above canopy, the majority of intensities are distributed among the Q2, Q3, and Q4 quadrants, with Q2 dominating (Fig. 21a-b.) During high water levels within the DEN canopy, Q3 and Q4 have the highest distribution, with Q4 dominating. Above the canopy, the majority of intensities are distributed equally in Q3 and Q4 quadrants. However, here, Q4 is slightly dominating. Additionally, we observed a consistent connection between quadrants Q1 and Q3 during both high and low water levels, except above the canopy during low water levels. However, the separation between Q1 and Q3 is less pronounced during low water levels above the canopy. (Fig. 21c-d.)

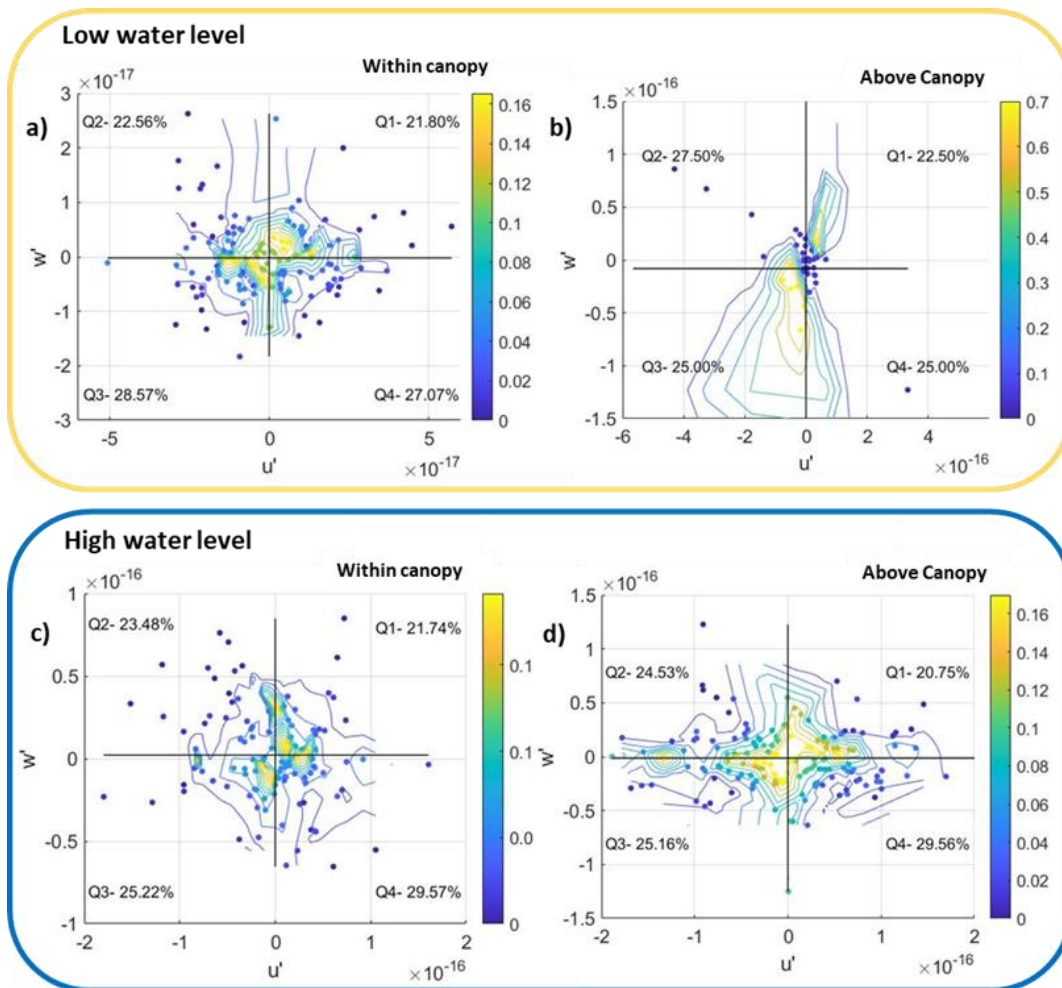


Figure 21. Quadrant analysis for DEN canopy observed during low water levels a) within and b) above the canopy and during high water levels c) within and d) above the canopy.

During high water levels within the H-DEN canopy, Q1 and Q4 have the highest distribution, with Q4 dominating. The majority of intensities are distributed in Q1 and Q3 quadrants, with Q1 slightly dominating above the canopy. Q1 and Q3 are linked together, similar to other canopy types within the canopy, while in the above the canopy, a clear separation can be observed (Fig. 22a-b)

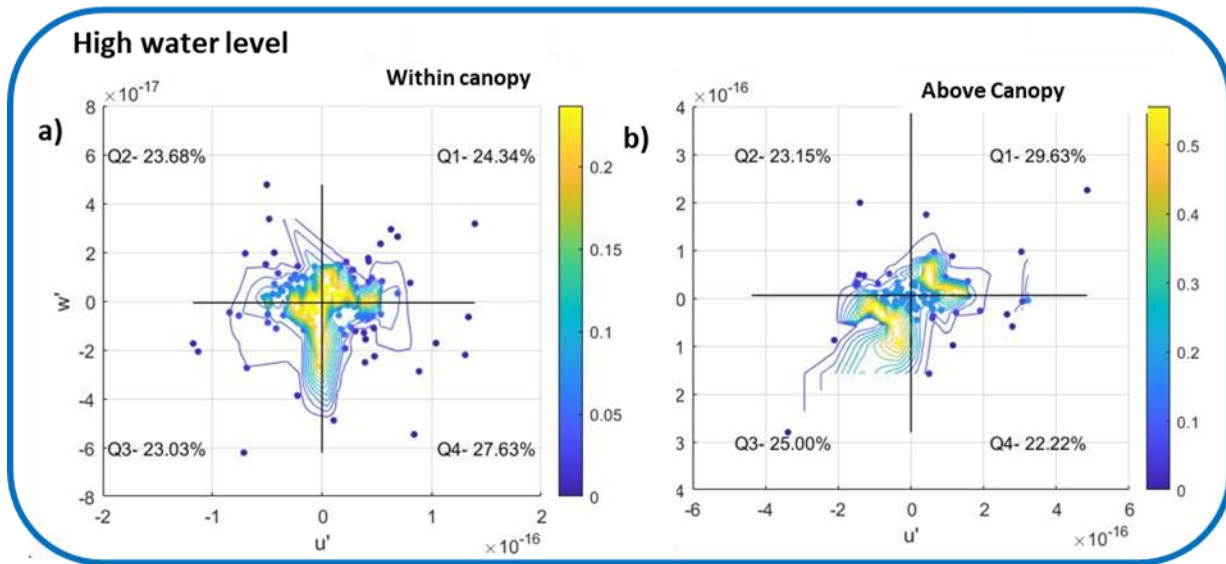


Figure 22. Quadrant analysis for H-DEN canopy observed during high water levels a) within and b) above the canopy.

Moreover, a general quadrant plot can be developed separately for all canopy types by combining relevant high water positions both within and above the canopy in order to identify the general difference among canopy types. Upon analyzing the combined quadrant plot for the SPA canopy, it is evident that the majority of turbulence intensities are concentrated around Q2 and Q3, indicating a prevalent sweeping motion, with Q3 slightly dominating (Fig. 23a). In the combined MOD canopy plot, the majority of turbulence intensities are concentrated around Q1 and Q4, with a sweeping motion towards the west slightly dominating (Fig. 23b). Similarly, for the DEN canopy, after combining relevant scenarios, it can be concluded that the majority of turbulence intensities are concentrated around Q3 and Q4, with a sweeping

motion towards the west slightly dominating (Fig. 23c). Combining all scenarios for the HDEN canopy, it can be observed that most turbulence intensities are concentrated around Q1 and Q4, with an ejecting motion towards the west slightly dominating (Fig. 23d). Notably, there is a clear separation of Q1 and Q3 observed in MOD and HDEN canopy combined quadrant plots compared to other canopy types. However, unlike the HDEN canopy, this pattern is not as clearly emergent in the MOD canopy when analyzed separately for different water levels and positions within and above the canopy, as shown in Fig. 20.

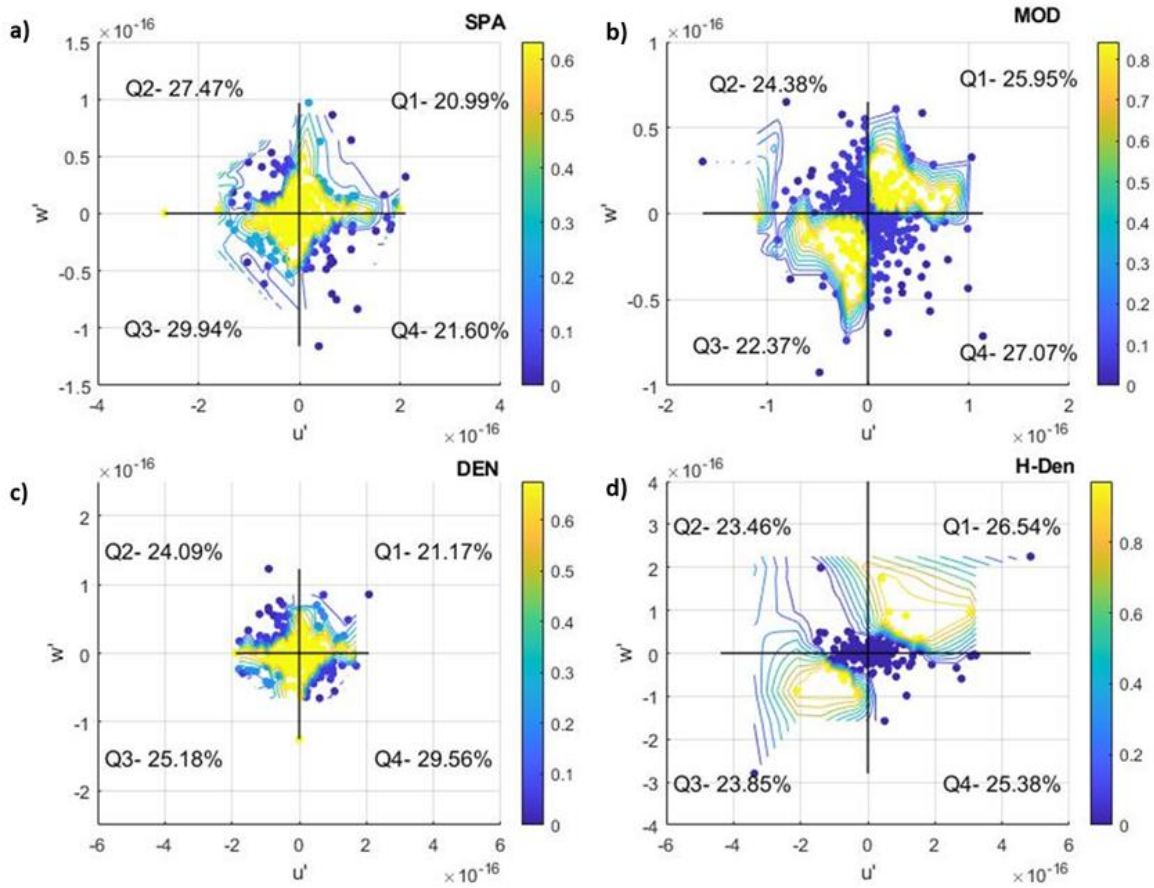


Figure 23. Combined quadrant plots for all the canopy types considering high water level and canopy position: a) SPA canopy, b) MOD canopy, c) DEN canopy, d) H-DEN Canopy.

Finally, the total contribution of Reynolds stress within each quadrant can be found by summing  $u'w'$  contributions, and it is observed that  $u'w'$  contributions are almost equally distributed among the four

quadrants. When comparing the contributions of Q1 and Q3 with respect to the other quadrants considering high and low water levels, within and above the canopy, a comprehensive Table 3 &4 can be obtained. Here, it can be observed that the Reynolds stress values are almost evenly distributed among the quadrants.

Table 3. Reynold stresses Distribution among the quadrants for High water level.

Above -High						
Canopy Type	Q1 +Q3	Q2 +Q4	Q1	Q2	Q3	Q4
SPA	48.23	51.76	24.28	19.56	23.95	32.2
MOD	43.32	56.66	25.08	30.5	18.24	26.16
DEN	49.61	50.39	27.96	27.42	21.65	22.97
H-DEN	50.38	49.62	28.3	39.24	22.08	10.38
Within -High						
Canopy Type	Q1 +Q3	Q2 +Q4	Q1	Q2	Q3	Q4
SPA	55.13	44.86	22.08	22.1	33.05	22.76
MOD	46.85	53.15	19.54	16.61	27.31	36.54
DEN	37.62	62.37	19.76	41.02	17.86	21.35
H-DEN	49.12	51.16	24.86	17.78	24.26	33.38

Table 4. Reynold stresses Distribution among the quadrants for Low water level.

Above -Low						
Canopy Type	Q1 +Q3	Q2 +Q4	Q1	Q2	Q3	Q4
SPA	56.25	43.74	21.06	24.93	35.19	18.81
MOD	48.58	51.41	13.4	23.77	35.18	27.64
DEN	46.1	53.9	9.25	21.9	36.85	32
Within -Low						
Canopy Type	Q1 +Q3	Q2 +Q4	Q1	Q2	Q3	Q4
SPA	29.93	70.07	11.17	27.11	18.76	42.96
MOD	42.23	57.77	25.47	27.6	16.76	30.17
DEN	48.15	51.84	22.95	31.79	25.2	20.05

## Sediment Analysis

Analysis of the core samples gathered along the reef transect (Fig. 24a) indicates that various sediment size classes are present. Utilizing the uniformity coefficient provides insight into the uniformity of the sediment. Particularly noteworthy is the variation in sediment distribution, ranging from non-uniform to well-graded, observed in the middle of the reef and along its slopes. Conversely, the outer regions of the reef exhibit a more uniform pattern (Fig. 24d). Upon analyzing the organic content, it was found to vary from location to location within the sediment cores. Generally, the organic content of the reef ranges from 22.8 g/kg to 86.2 g/kg (Fig. 24c).

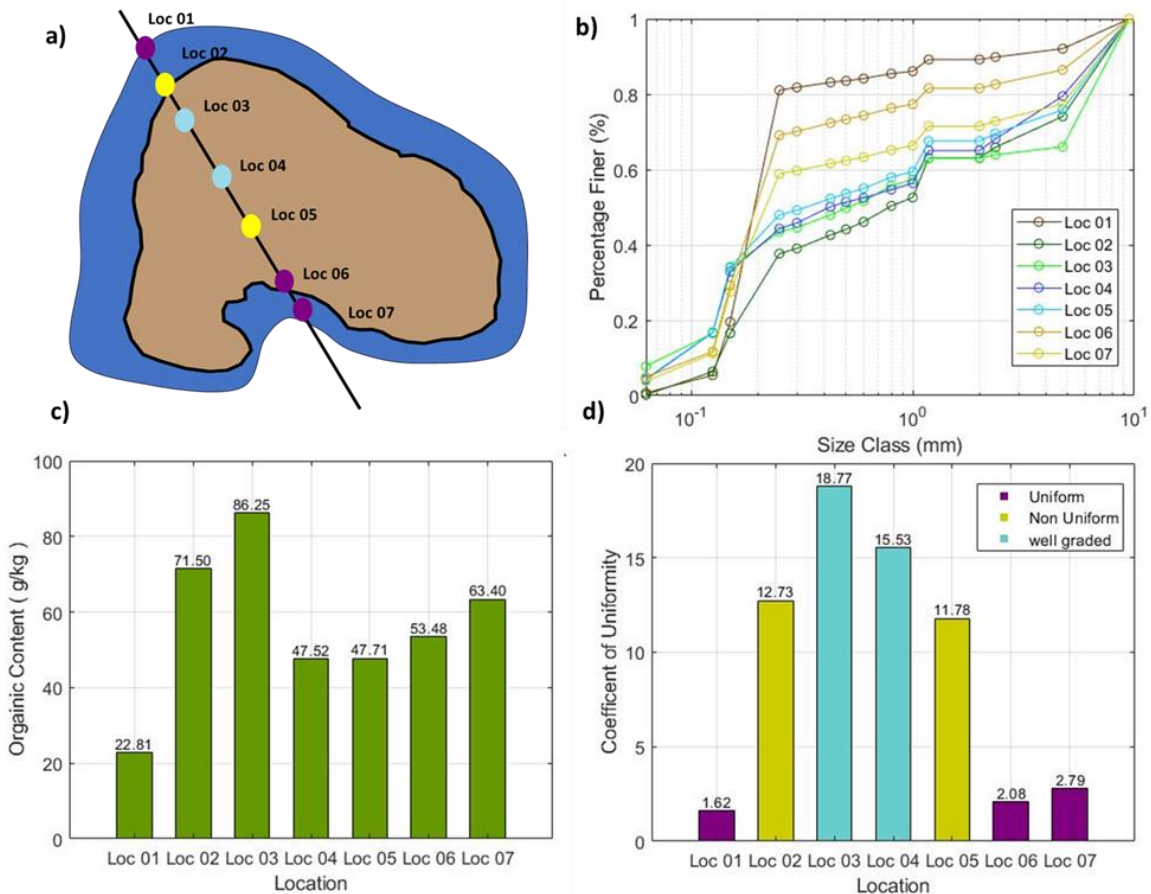


Figure 24. Variation in reef sediment characteristics: a) sediment core sample transect, b) grain size distribution, c) organic matter content, d) uniformity coefficient relevant to each bulk core sample.

## **CHAPTER FIVE: DISCUSSION**

This section primarily focuses on explaining the results obtained from the analysis, especially by providing appropriate interpretations with reference to existing literature. The discussion is divided into the following sections: General Parameters Analysis, Flow Attenuation, Turbulence Intensity, Drag Coefficients, Turbulence Production and Dissipation, Quadrant Analysis, Conclusion and Future Works. Flow attenuation results can be regarded as providing a macroscopic view of the intriguing phenomena behind the flow and various canopy interactions. Moving forward to discuss turbulence intensity, it will further expose their behavior by identifying patterns and relationships. Further exploration into turbulence dissipation and production parameters will help to quantify them more precisely. Additionally, quadrant plots will aid in visualizing their behavior and explaining certain phenomena more effectively.

### **General Parameters Analysis**

When analyzing the external parameters influencing the study site, such as water level, wind, and flow direction, it can be noted that throughout the experiment days, both during low and high-water levels, the wind blew from the Northeast direction to the Southwest direction. There wasn't a notable difference in wind speed among the experiment days of low and high-water levels. Furthermore, Weaver et al., (2016) suggested that Ekman forcing from the wind would be negligible in the Indian River Lagoon system, based on a research study conducted by Mied et al., (2010) on the Virginia coast reserve, due to the shared characteristics of the two systems. Hence It can be inferred that the impact of the wind on the study results may be minimal.

Water level increased gradually in channel and over the reef throughout the experiment . However, during high water levels, the water level increased with an increasing gradient, and during low water levels, it increased at a much lower gradient. Since all parameters were normalized in the analysis, the effect from the water level can be minimized. Moreover, when comparing the low water level and high water level experimental values, such as mean velocity and turbulent parameters, high water levels seem to have higher values, mainly due to the gradient difference of water levels for low and high water level experiments.

When analyzing stream flow direction (Fig. 8 -Results section), except for MOD within the canopy, in all other scenarios, the stream flow direction was from North-West to South-East, which is almost aligned with the study conducted by Weaver et al., (2016), who observed the flow direction of the entire Indian river lagoon system to be from North to South direction. However, within the MOD canopy layer, two main opposite flow directions can be observed. This can be explained by the canopy structure and density. In the MOD canopy, the cluster density is relatively low, allowing for less constraint on the flow compared to DENS or HDEN canopies. Hence, flow channels can be observed within the MOD canopy.

When considering the stream flow speed, MOD canopy exhibits the lowest mean speed during both high and low water levels compared to other canopies. This could be mainly due to the location of the MOD, situated in the middle of the reef, where the flow has already interacted with many canopies before reaching the measuring point of the MOD canopy, resulting in lower flow speeds.

## Flow Attenuation

Regarding water level, flow attenuation was generally higher during low water levels compared to high water levels. This difference can be attributed to the flow speeds; during low water levels, the overall water level was rising with a decreasing gradient, while during high water levels, it was rising with slightly higher gradients. Consequently, the results obtained during low water levels may not be sufficient to fully understand flow interactions with the canopy.

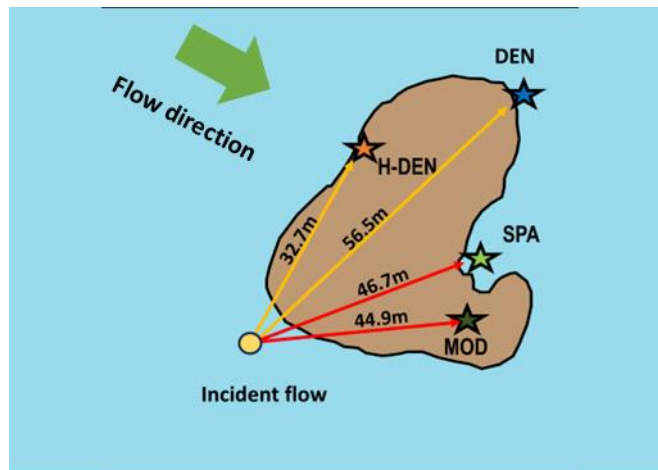


Figure 25. Distance from incident flow to canopy locations.

Within the canopy during high water levels, there was observed variability in flow attenuation among different canopy types, with MOD and SPA canopies exhibiting the highest attenuation. Moreover, the phenomenon of flow channeling within the MOD canopy can be another reason for the highest attenuation recorded within the canopy. The unique structure and arrangement of the MOD canopy may lead to the formation of distinct flow channels or pathways, causing the flow to be more constrained and encountering increased resistance as it moves through the canopy. This constrained flow within the MOD canopy can result in higher levels of attenuation compared to other canopy types where such flow channeling may not be as pronounced (Fig. 25).

Highwater level within the canopy, the lowest attenuation is recorded at DEN, which can be attributed to several reasons. Firstly, DEN is located at the edge of the reef close to the secondary channel, increasing the likelihood of interaction with secondary flows. This interaction can result in higher flow velocities compared to other locations, thus leading to lower attenuation. Additionally, the irregular arrangement of oysters within the DEN canopy (canopy height variability) may create flow channels or pathways with less obstruction. As water flows through these channels, it can accelerate due to reduced resistance compared to the more densely packed and ordered structure of the HDENS canopy.

Above the canopy at highwater level, there is interesting variation in flow attenuation. The lowest attenuation occurs in H-DEN, suggesting notably lower interaction above the canopy compared to DEN. This phenomenon can be explained by the flow over a boundary with multiple changes in roughness. The DEN canopy, with its varying roughness, creates disturbance layers that reduce overall flow velocity above the canopy. In contrast, the more uniform roughness of HDEN results in less frequent changes in disturbance layers and thus lower attenuation. Moreover, when comparing the drag coefficient ratio values for above and within the canopy for DEN and HDEN, they are 2.1 and 10.1 respectively (Fig. 18b-Results chapter). This disparity suggests a notable difference in drag force between above and within the H-DEN canopy. Such canopy discontinuity can lead to the creation of an inflection point in the velocity profile, where the profile resembles a free-shear-layer, as described by Luhar et al., (2008). This inflection point signifies a transition in flow behavior between the canopy and the free stream, indicating a complex interplay between the canopy structure and the surrounding flow dynamics.

Furthermore, focusing on boundary layer thickness can provide insight into these observations. The boundary layer is a thin layer of fluid adjacent to a surface where viscosity effects are notable. Near the surface, where the boundary layer occurs, fluid velocity is low, leading to the development of a pressure gradient that drives flow in the direction of low pressure. In H-DEN canopy above, flow velocity is accelerated due to the pressure gradient within the boundary layer, resulting in higher velocities compared

to the incident flow. However, in DEN above canopy, the varying canopy heights may induce turbulence, disrupting the development of the boundary layer and hindering flow acceleration. This turbulence can be likened to a completely rough bed, which further hinders the acceleration of flow above the canopy (Fig. 26).

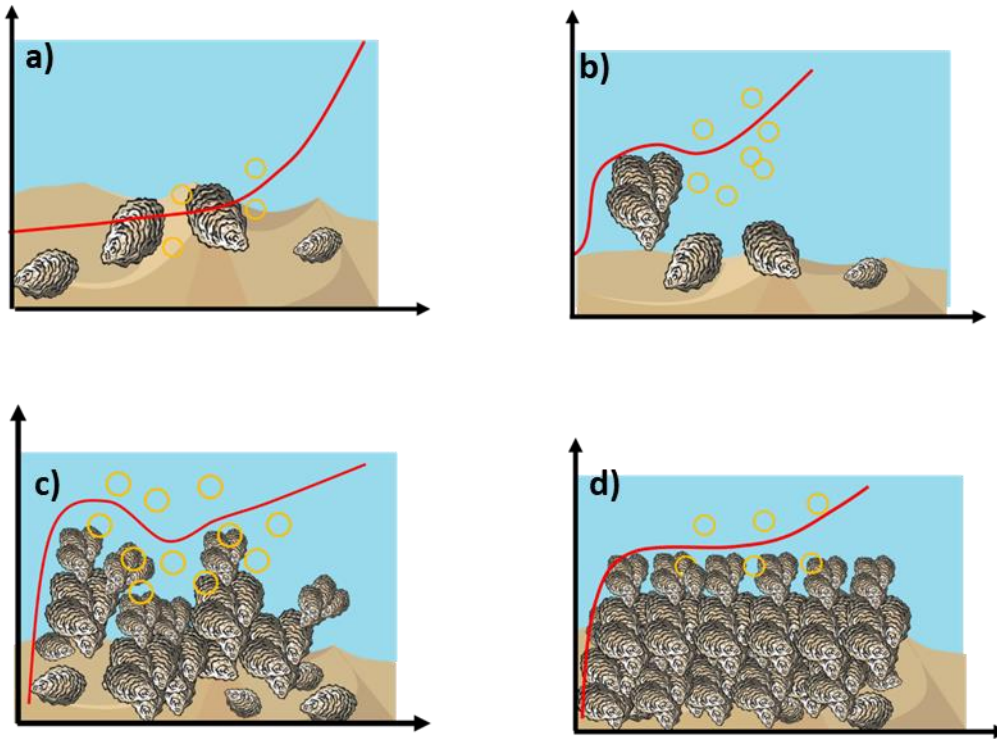


Figure 26. Development of boundary layer within the canopy types: a) SPA canopy, b) MOD canopy, c) DEN canopy, d) H-DEN canopy.

### **Turbulence Intensities:**

The highest turbulent intensity values, ranging between 2 and 7, are observed above the canopy of HDEN. In contrast, turbulent intensities in other canopy types typically range from 0 to 5. Notably, both above and below the SPA canopy, turbulent intensity records similar values, and during high water levels, the SPA canopy exhibits higher intensity values compared to both MOD and DEN canopy types.

When examining canopy turbulence intensity with the depth ratio, it is noted that MOD within the canopies of high and low water levels, and DEN within the low water level canopy, show higher intensities than above the canopy. Typically, higher intensity is expected above the canopy due to less obstruction to flow. Moreover, in the MOD (both high and low water levels) and low water level DEN canopies, intensity above the canopy occurs at a depth ratio higher than 0.2. According to literature, depth ratios less than 0.2 represent the wall region in unobstructed flows, where turbulence structure is mainly affected by wall or surface properties, and bursting phenomena usually occur here. In the depth ratio range of 0.2-0.6, known as the intermediate region, turbulence energy transforms into small-scale eddies, with limited production or dissipation (Nakagawa et al., 1975). While this analogy cannot be directly applied here due to canopy-induced flows, a noticeable similarity exists between the intermediate region in unobstructed flow and the canopy flow region within the same depth range.

Interestingly, in the high water level DENS canopy, both above and within, intensities fall under the wall region. Despite this, the DEN within canopy shows slightly lower intensity, due to higher drag force values. Comparing the drag coefficient ( $C_d$ ) values, DENS within the canopy have notably higher  $C_d$  than above, hindering the development of turbulent structures and leading to lower turbulence intensity within the canopy. Further when comparing the within and above  $C_d$  of HDEN canopy, the difference is even more pronounced than in the DEN canopy. Consequently, HDEN above the canopy exhibits higher intensity than within the canopy.

Moreover, due to the homogeneous canopy height in the HDEN canopy, a shear layer develops, accelerating fluid particles and intensifying turbulent mixing above the canopy. In contrast, the heterogeneity of canopy height in DEN and MOD canopies leads to the development of higher wakes and weakens the shear, resulting in less turbulent mixing compared to the HDEN canopy. This explains the lower range of turbulent intensities observed, especially during higher water levels in DEN and MOD canopies, relative to SPA and HDEN canopy types. However, during low water levels, this phenomenon is

not observed, with MOD and DEN within the canopy recording the highest mean intensity values, approximately 3.6 and 3 respectively. This is attributed to flow recirculation and restriction occurring at MOD and DEN canopies, leading to high turbulence within the canopy.

### **Drag Coefficient:**

The drag coefficient ( $C_d$ ) characterizes the force created by a fluid when moving around an object or surface. It can be considered a roughness measurement for the oyster canopy, providing insights into the physical surface arrangement of the canopy. This parameter can be used to delineate similarities and differences between various canopy types. Here, the drag coefficient is primarily calculated using the covariance method. The calculated drag coefficients ( $C_d$ ) for the SPA canopy align closely with the literature. Greenet al., (1998) reported  $C_d$  values for natural horse mussels ranging from 0.008 to 0.01, while Styles,(2015) observed  $C_d$  values ranging from 0.01 to 0.03 when measured from 10 cm above the eastern oyster bed. Kitsikoudis et al., (2020) found  $C_d$  coefficients for degraded and natural reefs varying within the range of 0.016 to 0.031 when measured 1 cm from the bed. However, these  $C_d$  values are subject to variability due to the method used for calculation and the location of canopy measurement. For example, Whitman & Reidenbach, (2012) observed a  $C_d$  of 0.019 at the top of the oyster canopy when measured 40 cm above the reef.  $C_d$  values for the MOD, DEN and H-DEN canopy are not found in the literature related to oyster canopies. Since this is the first study considering oyster canopy density heterogeneity, many researchers have not focused on measuring  $C_d$  based on canopy density, often measuring  $C_d$  at locations adjacent to the reef or on the reef regardless of canopy density.

Comparing  $C_d$  (Fig. 19a : Results chapter), it is noted that the DEN canopy creates almost similar drag as H-DEN canopy. This can be explained by the morphological differences between the canopies. The H-DEN canopy is almost box-shaped and cleanly cut, resulting in a clean separation of flow from its surface and stable wake patterns. In contrast, the random arrangement of clusters in the DEN and MOD canopy

introduces additional flow obstruction and form drag produced by flow over a spectrum of different-sized roughness elements, notably affecting velocity and boundary shear stress (Kean & Smith, 2006)

When comparing the canopy drag of MOD within and above, it's observed that above the canopy drag is higher than within the canopy. This can be explained by examining the structural arrangement of the MOD canopy. Unlike the denser DEN or H-DEN canopy, the MOD canopy consists of only a few clustered oyster shells, impacting the flow above the canopy and creating higher drag compared to within the canopy.

However, when comparing the within canopy  $C_d$  values of SPA and MOD canopy, they are almost identical. This suggests that the MOD canopy is a development of the SPA canopy with live clustered oysters. Furthermore, when comparing the  $C_d$  of MOD above and DEN within, and H-DEN canopy, they all fall within the range of 0.10-0.12. This suggests that the DEN and H-DEN canopy are developments of the MOD canopy with much more randomly and haphazardly arranged clusters, and systematically arranged clusters, respectively (Fig. 27).

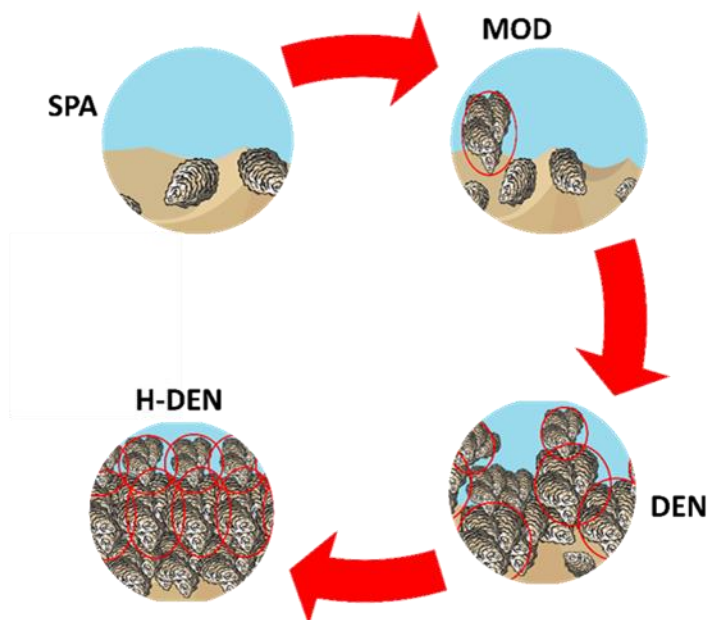


Figure 27. Evolutionary Traits in Oyster Reef Canopies. Comparison of canopy drag values illustrates how the MOD canopy exhibits traits of the SPA canopy, while the DEN and H-DEN canopies inherit characteristics from the MOD canopy.

Although the H-DEN canopy has a higher drag coefficient than all the canopy types, it doesn't result in notably higher turbulent intensities. This implies that drag coefficient isn't the sole governing factor for turbulence intensity; other factors like canopy roughness also play a role.

When comparing the  $C_d$  ratio for within and above, it is noted that H-DEN canopy have a notably higher ratio, equal to 10, while for the SPA and DEN canopy, it is almost equal to 2 and lower than H-DEN. This substantial drag difference in H-DEN may contribute to vertical stratification of flow velocities. The flow above the canopy may exhibit higher velocities and smoother flow conditions, while the flow within the canopy experiences slower velocities and greater turbulence due to vegetation-induced drag. This vertical stratification can affect the distribution of nutrients, oxygen, and other substances within the water column, impacting biological communities and ecosystem processes. This may explain the substantial large and healthy live oyster population observed in the H-DEN canopy compared to SPA, DEN and MOD

### **Turbulent Dissipation and Production:**

The distribution of turbulent dissipation and production across different canopy types and water levels reveals dynamic variations in turbulent parameters, highlighting the diverse energy transfer processes within these environments. Decreasing flow velocities correlate with elevated turbulent production levels, indicating intensified energy transfer.

In the SPA canopy, consistent patterns are observed for both production and dissipation during low water levels, but during high water levels, production exhibits greater fluctuations, especially towards the end of the flood tide. Above the canopy, dissipation remains constant while production decreases. In the MOD canopy, higher fluctuations are observed in both production and dissipation during low water levels, with dissipation remaining consistent during high water levels and production showing increased fluctuations, particularly with slow changes in water depth. Above the canopy, production dominates with higher fluctuations. Within the DEN canopy, dissipation remains consistent during low water levels, but increases

during high water levels, aligning with rising water depth, while production remains relatively steady. Above the canopy, dissipation dominates and gradually increases over time, with production showing more fluctuations. In the HDEN canopy, during high water levels, turbulent production and dissipation are consistent, but production is characterized by numerous fluctuations and intensified energy injection. Above the canopy, dissipation remains consistent, while production is accompanied by pronounced bursting phenomena, increasing towards the end of the flood tide as the change in water depth reduces.

When examining the turbulence production to dissipation ratio during low water levels, it becomes evident that turbulence dissipation is more prominent, with MOD and DEN canopies exhibiting the highest dissipation values, respectively.

In low water conditions, raw turbulent parameter values are lower in magnitude than during high water levels. This phenomenon was also observed when analyzing normalized turbulent intensity values. During high water levels, the highest intensities occur in MOD and DEN canopies, which are primarily governed by turbulent dissipation rather than production. Plotting turbulent production to dissipation ratios further illustrates that during high water levels, turbulent production dominates above all canopies except DENS and SPA. Within the canopy, all canopies except MOD and DEN exhibit higher turbulent production ratios (greater than 1). In low water levels, within the canopy, turbulent production only dominates in the SPA canopy, similar to high water levels within the canopy.

Researchers such as Kitsikoudis et al., (2020) observed higher turbulence production over dissipation in a natural reef and degraded reef 1 cm from the reef bed, and Pieterse et al., (2015) observed the same pattern when measuring flow velocity in a tidal channel. Furthermore, Cannon et al., (2022) observed turbulent production/dissipation ratios ranging from 3-4 in the above canopy of natural reef and restored reef when measured from approximately 9.5 cm from the bed. Moreover, Kitsikoudis et al., (2020) observed a somewhat balanced distribution of turbulence production to dissipation at the same natural

reef when measured data from 5 cm from the bed. Since authors have not accounted for the canopy arrangement and used different measurement heights, it is difficult to directly compare the turbulence dissipation and production results obtained with this study. However, when considering the magnitudes of turbulence production and dissipation, during high water levels, they are on the order of  $10^{-4} \text{ m}^2\text{s}^{-3}$  and during low water levels, they are on the order of  $10^{-6} \text{ m}^2\text{s}^{-3}$ . The high water level values are similar to values observed by Kitsikoudis et al., (2020) and Pieterse et al., (2015) but lower than the Styles, (2015) observed turbulent dissipation values, which were on the order of  $10^{-3} \text{ m}^2\text{s}^{-3}$ . Moreover, the low water level turbulence parameters were within the range of what Reidenbach et al., (2006) calculated, which was  $10^{-6} \text{ m}^2\text{s}^{-3} - 10^{-5} \text{ m}^2\text{s}^{-3}$ . Here, he calculated dissipation rate at 10 cm from a coral reef. Furthermore, when considering overall turbulence dissipation and production rates, the imbalanced nature was seen, and researchers such as Finnigan, (2000) and Reidenbach et al., (2007) also reported this discrepancy. The main cause of the imbalance between turbulence production and dissipation is the turbulence generated from the shear layer at the top of the canopy that penetrates the canopy Kitsikoudis et al., (2020)

Finally, when combining the turbulence information obtained from turbulence intensity values and dissipation values, it can be said that each type of canopy behaves as entirely different regions, both above and within the canopy. This factor can be further quantified based on turbulent dissipation and production. The given Fig. 28 illustrates the regions that can be observed within and above the canopy based on high water level turbulence intensity and production-to-dissipation ratio. Here, each canopy type has been divided into two separate regions, considering both above and within the canopy.

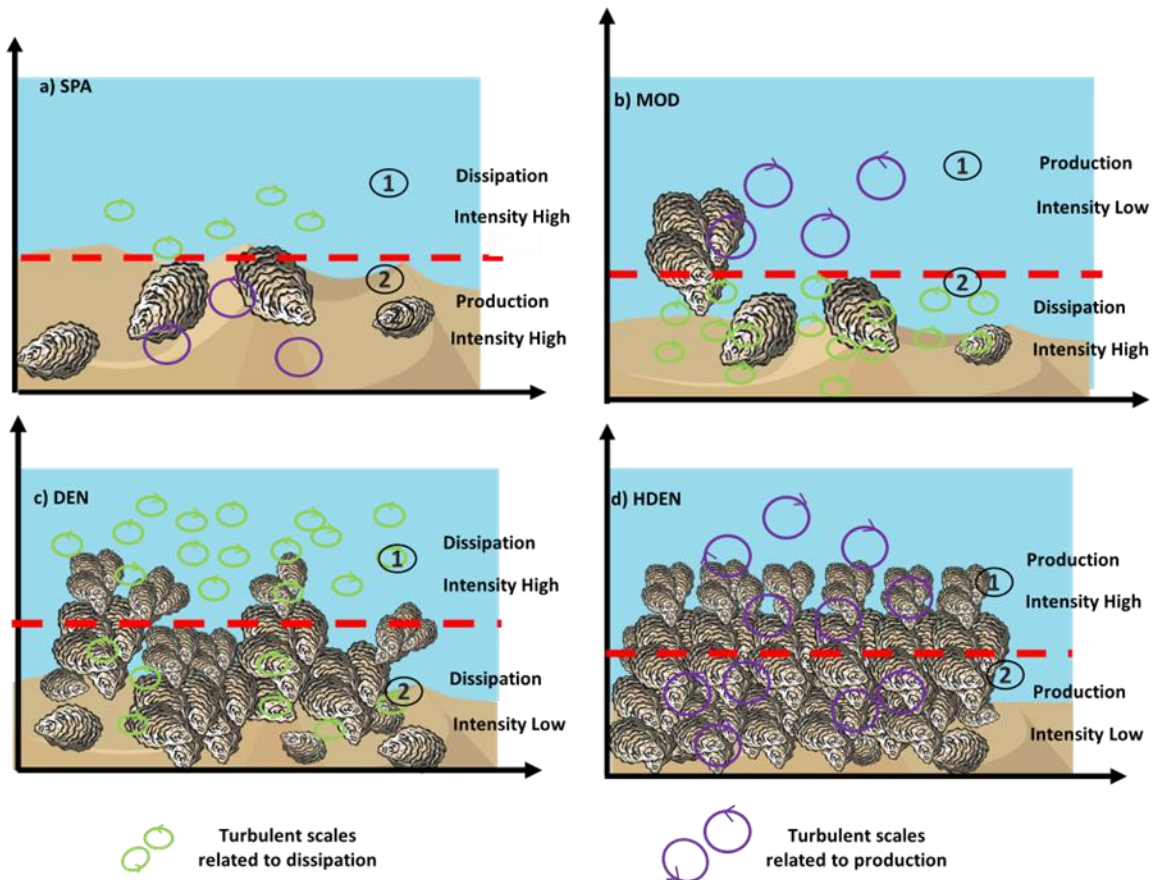


Figure 28. Canopy types divided into distinct regions based on the behavior of turbulence intensity, dissipation, and production values: a) SPA canopy, b) MOD canopy, c) DEN canopy, d) H DEN canopy.

### Quadrant Analysis:

Diversity in flow behavior and turbulent fluctuations, in terms of ejection and sweeping motions, can be visualized through quadrant analysis, and developed contour plots considering their probability distribution. Wallace et al., (1972) conducted the first quadrant analysis for Reynolds stress, and later, it has been recognized the importance of recognizing the sign of the velocity fluctuation when analyzing turbulent behavior. Typically, in the literature, the sign of the velocity fluctuation is classified into 4 quadrants ( $Q1(u, v)$ ,  $Q2(-u, -v)$ ,  $Q3(-u, -v)$ , and  $Q4(u, -v)$ ). Q2 and Q4 quadrants are considered as

ejection and sweeping, while Q1 and Q3 are called outward and inward motions, respectively (Corinop & Brodkey, 1969; Wallace et al., 1972; Wallace, 2016)

However, here, the definition of ejection and sweeping events is based on the dominant direction of the instantaneous velocity fluctuation (Dimas et al., 2016). When the stream flow is aligned with the +u direction, Q2 and Q4 quadrants are considered as ejection and sweeping, and if it is aligned with the -u direction, Q1 and Q3 quadrants are considered as ejection and sweeping, respectively. Hence, in this study, based on the flow analysis, the dominant flow direction is towards the -u direction, so Q1 and Q3 represent ejection and sweeping motion, respectively. Ejection events involve the expulsion of low-speed fluid parcels into higher-speed regions, while sweeping events involve the transport of high-speed fluid across lower-speed regions.

When observing the Reynolds stress within the quadrants, the values are almost evenly distributed among the quadrants. In DEN and MOD canopies, the total contribution of Q1 and Q3 is slightly lower than that of Q2 and Q4. However, Reidenbach et al. (2012) observed greatly imbalanced behavior among the quadrants, such as Q1 (8%), Q2 (33%), Q3 (7%), and Q4 (51%), showing a greater tendency towards sweeping motion on a mature oyster reef. They also observed a balanced behavior in Reynolds stress values on a restored oyster reef, such as Q1 (16%), Q2 (35%), Q3 (14%), and Q4 (35%). However, in this study, such patterns were not generally observed except in the DEN within the canopy at high water level, where the dominant quadrants shifted to Q2 and Q4, with Q2 having more than 40% of the Reynolds stress, implying that ejection motion is dominating.

In summary, it can be said that except for DEN within the canopy, the Reynolds stress distribution is almost equally distributed. This implies that canopy structure notably impacts turbulent fluctuations and leads to enhanced mixing and redistribution of momentum.

## Conclusion

In conclusion, each canopy type contributes uniquely to reef development and influences overall flow dynamics. Analysis of highwater level attenuation patterns revealed distinct attenuation behaviors, indicating varying responses to incident flow. Specifically, the SPA canopy exhibited attenuation levels ranging from 48% to 70%, while the MOD canopy ranged from 64% to 96%, and the DEN canopy ranged from 64% to 90%. Notably, the H-DEN canopy displayed negative attenuation values, suggesting distinctive canopy behavior patterns. Moreover, sediment analysis revealed spatial heterogeneity within the reef, with varying sediment classes (0 to 10 mm) and organic content (22.8 to 86.2 g/kg) throughout the study area. This underscores the reef's multifaceted nature, behaving combination of subsystems.

From the canopy scale turbulence analysis, it is evident that higher levels of turbulent mixing occur in the DEN canopy above the canopy and MOD canopy within the canopy. Turbulent intensity values range from 0 to 30 in these cases, distinctly standing out from the rest of the canopies, which range from 0 to 5. This disparity can be attributed to the uneven nature of the canopy arrangement and its interaction with turbulence. This observation is supported by the turbulent dissipation, and quadrant analysis results. Furthermore, it is noteworthy that turbulent dissipation is prominent in all the highest turbulent mixing events, with the DEN above and MOD within the canopy recording turbulent production to dissipation ratio values of 0.82 and 0.88 respectively.

When considering MOD and DEN canopies in terms of canopy density, it is noted that MOD canopy has a lower density of live clusters compared to DEN. This could be attributed to the high level of turbulent mixing within the MOD canopy layer, potentially hindering larval settlement by disrupting their swimming patterns and attachment abilities. Additionally, the lack of vertical canopy structures in the MOD layer may deter oyster larvae from residing in the canopy. Conversely, in the DEN canopy, the highest turbulent mixing occurs above the canopy, creating an ideal environment for larval settlement within the canopy

due to reduced turbulence. This allows for oyster larvae to attach to the within the canopy of the DEN layer. Moreover, the higher level of mixing in the above canopy penetrates nutrients, oxygen, and other substances within the water column, promoting an ideal environment for oyster larvae to settle down. In the H-DEN above the canopy, intense turbulent mixing is observed. However, due to the canopy's uniform shape, it promotes a shear layer above the canopy, which promotes vortex shredding in the wake region above the canopy and leading to turbulence production dominance. This affects the dynamics of ejection and sweeping motions within the turbulent boundary layer. As observed in the quadrant plot, these motions are properly organized and ordered, resulting in a balanced distribution of nutrients and other substances within the canopy. Consequently, oyster larvae tend to grow and flourish more densely than in other canopy types.

When comparing the drag coefficient values, the highest values were obtained for the DEN and H-DEN canopies, falling within the range of 0.11-0.12. Despite sharing similar numerical ranges, these canopies exhibit distinct turbulent characteristics attributed to their morphological arrangements. Specifically, the DEN canopy displays varying canopy heights, while the H-DEN canopy features uniform heights. Moreover, when comparing within and above canopy types, clear differences emerge, underscoring the subtle nature of each canopy. This observation supports the concept that each canopy can be further subdivided into regions such as within and above, each exhibiting different turbulent parameters. Such findings emphasize the complexity and heterogeneity inherent in canopy structures.

Overall, finding of this research study suggest there is potential to optimize reef growth and functionality by manipulating flow regimes, which could pave the way for enhanced artificial reef development. Further research in this area could explore the specific mechanisms driving turbulent mixing within different canopy types and how they impact larval settlement and reef development.

## **Future Work**

Future research endeavors should prioritize the detailed examination of each canopy type within oyster reef ecosystems, researching into specific aspects such as sediment transport dynamics. By conducting comprehensive sediment transport studies, researchers can understand the distinct influence of each canopy type on sediment movement and deposition. Furthermore, investigating nutrient levels, including oxygen concentration, nitrogen concentration, and carbon content, across different canopy types is essential. Such analyses will shed light on the underlying factors contributing to variations in canopy density within oyster reefs. By unraveling the intricate relationship between nutrient availability and canopy density, researchers can unravel key mechanisms shaping the structural diversity of oyster reef canopies. In addition, it is imperative to explore canopy transition zones within oyster reefs to decipher the intricate flow dynamics associated with changes in canopy density. This investigation will offer valuable insights into how variations in canopy density influence flow patterns and nutrient distributions within reef ecosystems. By learning the dynamics of canopy transitions, researchers can gain a deeper understanding of the spatial heterogeneity within oyster reefs and its implications for ecosystem function.

## APPENDIX: REEF LASER SCAN ANALYSIS FOR CANOPY HEIGHT

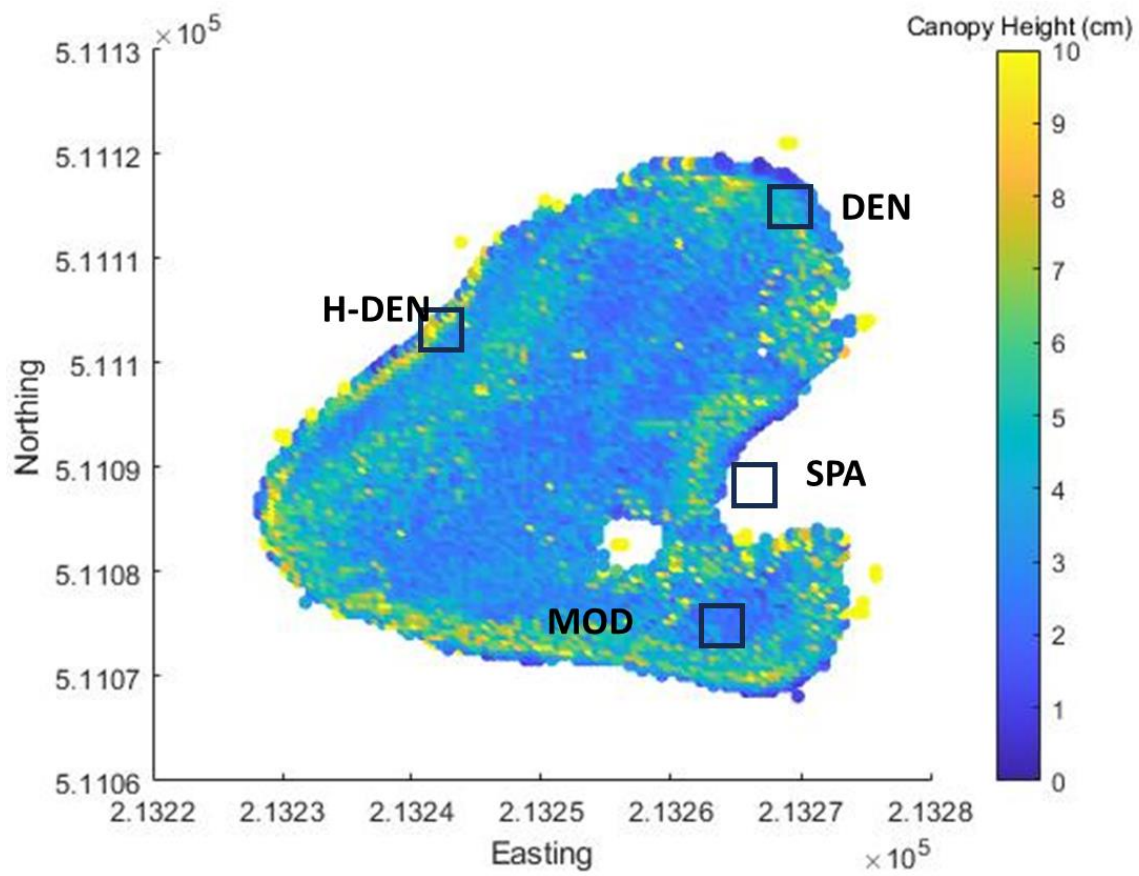


Figure 29. Laser Scan Analysis for Study site.

## LIST OF REFERENCES

- ASTM. (2006). *Standard test method for sieve analysis of fine and coarse aggregates*.
- ASTM. (2013). *Standard Test Method for Materials Finer than 75- $\mu$ m (No. 200) Sieve in Mineral Aggregates by Washing*.
- Bahr, L. M. (1976). Energetic Aspects of the Intertidal Oyster Reef Community at Sapelo Island, Georgia (USA) ENERGETIC ASPECTS OF THE INTERTIDAL OYSTER REEF COMMUNITY AT SAPELO ISLAND, GEORGIA (USA)'. In *Source: Ecology* (Vol. 57, Issue 1).
- Bahr, L. M., & Lanier, W. P. (1981). *The ecology of intertidal oyster reefs of the South Atlantic coast: A community profile*. U. S. Fish and Wildlife Service.  
<https://www.researchgate.net/publication/353298818>
- Bartol, I. K., & Mann, R. (1999). *Small-Scale Patterns of Recruitment On A Constructed Intertidal Reef: The Role of Spatial Refugia* (Vol. 88). VIMS Books and Book Chapters.  
<https://scholarworks.wm.edu/vimsbooks/88>
- Bartol, I. K., Mann, R., & Luckenbach, M. (1999). Growth and mortality of oysters (*Crassostrea virginica*) on constructed intertidal reefs: effects of tidal height and substrate level. In *Journal of Experimental Marine Biology and Ecology* (Vol. 237).
- Bertness, M. D., Gaines, S. D., & Yeh, S. M. (1998). Making Mountains out of Barnacles: The Dynamics of Acorn Barnacle Hummocking. *Ecology*, 79(4), 1382. <https://doi.org/10.2307/176750>
- Bilkovic, D. M., Mitchell, M., Mason, P., & Duhring, K. (2016). The Role of Living Shorelines as Estuarine Habitat Conservation Strategies. *Coastal Management*, 44(3), 161–174.  
<https://doi.org/10.1080/08920753.2016.1160201>

- Bishop, M. J., & Peterson, C. H. (2006). *Direct Effects of Physical Stress Can Be Counteracted by Indirect Benefits: Oyster Growth on a Tidal Elevation Gradient* (Vol. 147, Issue 3).
- Bobo, M. Y., Richardson, D. L., Coen, L. D., & Burrell, V. G. (1997). *A REPORT ON THE PROTOZOAN PATHOGENS PERKINSUS MARINUS (DERMO) AND HAPLOSPORIDIUM NELSONI (MSX) IN SOUTH CAROLINA SHELLFISH POPULATIONS, WITH AN OVERVIEW OF THESE SHELLFISH PATHOGENS PREPARED BY.*
- Borsje, B. W., van Wesenbeeck, B. K., Dekker, F., Paalvast, P., Bouma, T. J., van Katwijk, M. M., & de Vries, M. B. (2011). How ecological engineering can serve in coastal protection. In *Ecological Engineering* (Vol. 37, Issue 2, pp. 113–122). <https://doi.org/10.1016/j.ecoleng.2010.11.027>
- Bouma, T. J., van Belzen, J., Balke, T., Zhu, Z., Airoidi, L., Blight, A. J., Davies, A. J., Galvan, C., Hawkins, S. J., Hoggart, S. P. G., Lara, J. L., Losada, I. J., Maza, M., Ondiviela, B., Skov, M. W., Strain, E. M., Thompson, R. C., Yang, S., Zanuttigh, B., ... Herman, P. M. J. (2014). Identifying knowledge gaps hampering application of intertidal habitats in coastal protection: Opportunities & steps to take. *Coastal Engineering*, 87, 147–157. <https://doi.org/10.1016/j.coastaleng.2013.11.014>
- Bricker, J. D., & Monismith, S. G. (2007). Spectral wave-turbulence decomposition. *Journal of Atmospheric and Oceanic Technology*, 24(8), 1479–1487. <https://doi.org/10.1175/JTECH2066.1>
- Brown, B. L., Butt, A. J., Meritt, D., & Paynter, K. T. (2005). Evaluation of resistance to Dermo in eastern oyster strains tested in Chesapeake Bay. *Aquaculture Research*, 36(15), 1544–1554. <https://doi.org/10.1111/j.1365-2109.2005.01377.x>
- Burrell, V. G. (1986). *Species Profiles: Life Histories and Environmental Requirements of Coastal Fishes and Invertebrates (South Atlantic): American oyster Item Type monograph.* <http://hdl.handle.net/1834/21292>

- Byers, J. E., Grabowski, J. H., Piehler, M. F., Hughes, A. R., Weiskel, H. W., Malek, J. C., & Kimbro, D. L. (2015a). Geographic variation in intertidal oyster reef properties and the influence of tidal prism. *Limnology and Oceanography*, *60*(3), 1051–1063. <https://doi.org/10.1002/lno.10073>
- Byers, J. E., Grabowski, J. H., Piehler, M. F., Hughes, A. R., Weiskel, H. W., Malek, J. C., & Kimbro, D. L. (2015b). Geographic variation in intertidal oyster reef properties and the influence of tidal prism. *Limnology and Oceanography*, *60*(3), 1051–1063. <https://doi.org/10.1002/lno.10073>
- Cannon, D. J., Kibler, K. M., Taye, J., & Medeiros, S. C. (2023). Characterizing canopy complexity of natural and restored intertidal oyster reefs (*Crassostrea virginica*) with a novel laser-scanning method. *Restoration Ecology*, *31*(7). <https://doi.org/10.1111/rec.13973>
- Cannon, D., Kibler, K. M., Kitsikoudis, V., Medeiros, S. C., & Walters, L. J. (2022). Variation of mean flow and turbulence characteristics within canopies of restored intertidal oyster reefs as a function of restoration age. *Ecological Engineering*, *180*. <https://doi.org/10.1016/j.ecoleng.2022.106678>
- Chang, K., & Constantinescu, G. (2015). Numerical investigation of flow and turbulence structure through and around a circular array of rigid cylinders. *Journal of Fluid Mechanics*, *776*, 161–199. <https://doi.org/10.1017/jfm.2015.321>
- Coen, L. D., Knott, D. M., Wenner, E. L., Hadley, N. H., Ringwood, A. H., & Bobo, M. Y. (1999). Intertidal Oyster Reef Studies in South Carolina: Design, Sampling and Experimental Focus for Evaluating Habitat Value and Function. In *Marine Science Press*. Marine Science Press. <https://doi.org/10.21220/V5NK51>
- Colden, A. M., Fall, K. A., Cartwright, G. M., & Friedrichs, C. T. (2016). Sediment Suspension and Deposition Across Restored Oyster Reefs of Varying Orientation to Flow: Implications for Restoration. *Estuaries and Coasts*, *39*(5), 1435–1448. <https://doi.org/10.1007/s12237-016-0096-y>

- Corinop, E. €2, & Brodkey, R. S. (1969). A visual investigation of the wall region in turbulent flow. In *J. Fluid Mech* (Vol. 37, Issue 1).
- Crosby, M. P., Roberts, C. F., & Kenny, P. D. (1991). Effects of immersion time and tidal position on in situ growth rates of naturally settled eastern oysters, *Crassostrea virginica* (Gmelin, 1791). *J. Shellfish Res*, 10, 95–103.
- Dame, R. F. (1996). *Ecology of bivalves: an ecosystem approach*. CRC Press.
- Dame, R. F., & Patten, B. C. (1981). Analysis of Energy Flows in an Intertidal Oyster Reef. *Marine Ecology Progress Series*, 5(2), 115–124.
- Dame, R. F., Spurrier, J. D., & Wolaver, T. G. (1989). Carbon, nitrogen and phosphorus processing by an oyster reef. *MARINE ECOLOGY PROGRESS SERIES Mar. Ecol. Prog. Ser*, 54, 249–256.
- Dame, R. F., Wolaver, T. G., & Libes, S. M. (1985). The summer uptake and release of nitrogen by an intertidal oyster reef. *Netherlands Journal of Sea Research*, 19(3–4), 265–268.  
[https://doi.org/10.1016/0077-7579\(85\)90032-8](https://doi.org/10.1016/0077-7579(85)90032-8)
- Donnelly, J. P., Cleary, P., Newby, P., & Ettinger, R. (2004). Coupling instrumental and geological records of sea-level change: Evidence from southern New England of an increase in the rate of sea-level rise in the late 19th century. *Geophysical Research Letters*, 31(5). <https://doi.org/10.1029/2003gl018933>
- Down, C., & Withrow, R. (1978). *Vegetation and other parameters in the Brevard County bar-built estuaries*. <https://ntrs.nasa.gov/citations/19790011257>
- Drexler, M., Parker, M. L., Geiger, S. P., Arnold, W. S., & Hallock, P. (2014). Biological Assessment of Eastern Oysters (*Crassostrea virginica*) Inhabiting Reef, Mangrove, Seawall, and Restoration Substrates. *Estuaries and Coasts*, 37(4), 962–972. <https://doi.org/10.1007/s12237-013-9727-8>

Finnigan, J. (2000). TURBULENCE IN PLANT CANOPIES. In *Annu. Rev. Fluid Mech* (Vol. 32).

[www.annualreviews.org](http://www.annualreviews.org)

Fodrie, F. J., Rodriguez, A. B., Baillie, C. J., Brodeur, M. C., Coleman, S. E., Gittman, R. K., Keller, D. A.,

Kenworthy, M. D., Poray, A. K., Ridge, J. T., Theuerkauf, E. J., & Lindquist, N. L. (2014). Classic paradigms in a novel environment: Inserting food web and productivity lessons from rocky shores and saltmarshes into biogenic reef restoration. *Journal of Applied Ecology*, 51(5), 1314–1325.

<https://doi.org/10.1111/1365-2664.12276>

Fuchs, H. L., Hunter, E. J., Schmitt, E. L., & Guazzo, R. A. (2013). Active downward propulsion by oyster larvae in turbulence. *Journal of Experimental Biology*, 216(8), 1458–1469.

<https://doi.org/10.1242/jeb.079855>

Goring, D. G., & Nikora, V. I. (2002). *Despiking Acoustic Doppler Velocimeter Data*.

<https://doi.org/10.1061/ASCE0733-94292002128:1117>

Grabowski, J. H., Hughes, A. R., Kimbro, D. L., & Dolan, M. A. (2005). HOW HABITAT SETTING INFLUENCES RESTORED OYSTER REEF COMMUNITIES. In *Ecology* (Vol. 86, Issue 7).

Grave, C. (1905). *Investigations for the promotion of the oyster industry of North Carolina. Report of the U.S. Commercial Fisheries*.

Green, M. O., Hewitt, J. E., & Thrush, S. F. (1998). Seabed drag coefficient over natural beds of horse mussels (*Atrina zelandica*). *Journal of Marine Research*, 56, 613–637.

<https://elischolar.library.yale.edu/>.

Grizzle, R. E. (1990). *Distribution and abundance of Crassostrea virginica (Gmelin, 1791) (Eastern oyster) and Mercenaria spp. (Quahogs) in a coastal lagoon*.

<https://www.researchgate.net/publication/312979216>

- Grizzle, R., Ward, K., Geselbracht, L., & Birch, A. (2018). Distribution and Condition of Intertidal Eastern Oyster (*Crassostrea virginica*) Reefs in Apalachicola Bay Florida Based on High-Resolution Satellite Imagery. *Journal of Shellfish Research*, 37(5), 1027–1038. <https://doi.org/10.2983/035.037.0514>
- Hansen, J. C. R., & Reidenbach, M. A. (2017). Turbulent mixing and fluid transport within Florida Bay seagrass meadows. *Advances in Water Resources*, 108, 205–215. <https://doi.org/10.1016/j.advwatres.2017.08.001>
- Hargis, W. J. (1999). *Chesapeake Oyster Reefs, Their Importance, Destruction and Guidelines for Restoring Them*. <https://scholarworks.wm.edu/vimsbooks/92>
- Haven, D. S., & Morales-Alamo, R. (1966). Aspects of Biodeposition By Oysters and Other Invertebrate Filter Feeders. *Limnology and Oceanography*, 11(4), 487–498. <https://doi.org/10.4319/lo.1966.11.4.0487>
- Hitzegrad, J., Brohmann, L., Pfennings, K., Hoffmann, T. K., Eilrich, A. K., Paul, M., Welzel, M., Schlurmann, T., Aberle, J., Wehrmann, A., & Goseberg, N. (2022). Oyster Reef Surfaces in the Central Wadden Sea: Intra-Reef Classification and Comprehensive Statistical Description. *Frontiers in Marine Science*, 9. <https://doi.org/10.3389/fmars.2022.808018>
- Hogan, S., & Reidenbach, M. A. (2019). Quantifying and mapping intertidal oyster reefs utilizing LiDAR-based remote sensing. *Source: Marine Ecology Progress Series*, 630, 83–99. <https://doi.org/10.2307/26920542>
- Hubbard, A. B., & Reidenbach, M. A. (2015). Effects of larval swimming behavior on the dispersal and settlement of the eastern oyster *Crassostrea virginica*. *Marine Ecology Progress Series*, 535, 161–176. <https://doi.org/10.3354/meps11373>

- Kastner-Klein, P., & Rotach, M. W. (2004). *MEAN FLOW AND TURBULENCE CHARACTERISTICS IN AN URBAN ROUGHNESS SUBLAYER*.
- Kean, J. W., & Smith, J. D. (2006). Form drag in rivers due to small-scale natural topographic features: 2. Irregular sequences. *Journal of Geophysical Research: Earth Surface*, *111*(4).  
<https://doi.org/10.1029/2006JF000490>
- Kennedy, V. S., Newell, R. I. E., Eble, A. F., & Maryland Sea Grant College. (1996). *The eastern oyster : Crassostrea virginica*. Maryland Sea Grant College.
- Kibler, K. M., Kitsikoudis, V., Donnelly, M., Spiering, D. W., & Walters, L. (2019). Flow-vegetation interaction in a living shoreline restoration and potential effect to mangrove recruitment. *Sustainability (Switzerland)*, *11*(11). <https://doi.org/10.3390/su11113215>
- Kim, S.-C., Friedrichs, C. T., Maa, J. P.-Y., & Wright, L. D. (2000). Estimating Bottom Stress in Tidal Boundary Layer from Acoustic Doppler Velocimeter Data. *Journal of Hydraulic Engineering*, *126*(6), 399–406.  
[https://doi.org/10.1061/\(asce\)0733-9429\(2000\)126:6\(399\)](https://doi.org/10.1061/(asce)0733-9429(2000)126:6(399))
- Kitsikoudis, V., Kibler, K. M., & Walters, L. J. (2020). In-situ measurements of turbulent flow over intertidal natural and degraded oyster reefs in an estuarine lagoon. *Ecological Engineering*, *143*.  
<https://doi.org/10.1016/j.ecoleng.2019.105688>
- Kitsikoudis, V., Yagci, O., Kirca, V. S. O., & Kellecioglu, D. (2016). Experimental investigation of channel flow through idealized isolated tree-like vegetation. *Environmental Fluid Mechanics*, *16*(6), 1283–1308. <https://doi.org/10.1007/s10652-016-9487-7>
- Kraeuter, J. N., Ford, S., & Cummings, M. (2007). Oyster growth analysis: A comparison of methods. *Journal of Shellfish Research*, *26*(2), 479–491. [https://doi.org/10.2983/0730-8000\(2007\)26\[479:OGAACO\]2.0.CO;2](https://doi.org/10.2983/0730-8000(2007)26[479:OGAACO]2.0.CO;2)

- Lenihan, H. S. (1999a). Physical-Biological Coupling on Oyster Reefs: How Habitat Structure Influences Individual. In *Source: Ecological Monographs* (Vol. 69, Issue 3).  
<http://www.jstor.org>URL:<http://www.jstor.org/stable/2657157>Accessed:02-12-201509:58UTC
- Lenihan, H. S. (1999b). Physical-biological coupling on oyster reefs: How habitat structure influences individual performance. *Ecological Monographs*, 69(3), 251–275. [https://doi.org/10.1890/0012-9615\(1999\)069\[0251:PBCOOR\]2.0.CO;2](https://doi.org/10.1890/0012-9615(1999)069[0251:PBCOOR]2.0.CO;2)
- Lenihan, H. S., & Peterson, C. H. (1998). How habitat degradation through fishery disturbance enhances impacts of hypoxia on oyster reefs. *Ecological Applications*, 8(1), 128–140.  
[https://doi.org/10.1890/1051-0761\(1998\)008\[0128:HHDTFD\]2.0.CO;2](https://doi.org/10.1890/1051-0761(1998)008[0128:HHDTFD]2.0.CO;2)
- Lu, S., & Willmarth WW. (1973). Measurements of the structure of the Reynolds stress in a turbulent boundary layer. *Journal of Fluid Mechanics*, 481–511.  
<https://doi.org/doi:10.1017/S0022112073000315>
- Luhar, M., Rominger, J., & Nepf, H. (2008). Interaction between flow, transport and vegetation spatial structure. *Environmental Fluid Mechanics*, 8(5–6), 423–439. <https://doi.org/10.1007/s10652-008-9080-9>
- Mackenzie, C. L. (1983). To Increase Oyster Production in the Northeastern United States. *Marine Fisheries Review*.
- Mackenzie, C. L. (1996). History of Oystering in the United States and Canada, Featuring the Eight Greatest Oyster Estuaries. *Marine Fisheries Review*.
- Malek, J. C., & Breitburg, D. (2010). *Title of thesis: THE EFFECTS OF INTERTIDAL EXPOSURE ON DISEASE, MORTALITY, AND GROWTH OF THE EASTERN OYSTER, CRASSOSTREA VIRGINICA*. Univ. of Maryland.
- Michael Risk. (1972). *FISH DIVERSITY ON A CORAL REEF IN THE VIRGIN ISLANDS*.

- Mied, R. P., Schulz, W. J., Handler, R. A., Snow, C. M., Fusina, R. A., & Porter, J. H. (2010). Remote and local forcing of a coastal lagoon: The Virginia Coast Reserve. *Continental Shelf Research*, 30(20), 2057–2066. <https://doi.org/10.1016/j.csr.2010.10.005>
- Nakagawa, H., Nezu, I., & Ueda, H. (1975). *TURBULENCE OF OPEN CHANNEL FLOW OVER SMOOTH AND ROUGH BEDS*.
- Nelson, K. A., Leonard, L. A., Posey, M. H., Alphin, T. D., & Mallin, M. A. (2004). Using transplanted oyster (*Crassostrea virginica*) beds to improve water quality in small tidal creeks: A pilot study. *Journal of Experimental Marine Biology and Ecology*, 298(2), 347–368. [https://doi.org/10.1016/S0022-0981\(03\)00367-8](https://doi.org/10.1016/S0022-0981(03)00367-8)
- Newell, R. I. (1988). Ecological changes in Chesapeake Bay: are they the result of overharvesting the American oyster, *Crassostrea virginica* ? *Understanding the Estuary: Advances in Chesapeake Bay Research*, 536–546.
- Nezu, I. (1977). *TURBULENT STRUCTURE IN OPEN-CHANNEL FLOWS*.
- Pentland, A. P. (1984). Fractal-Based Description of Natural Scenes. In *IEEE TRANSACTIONS ON PATTERN ANALYSIS AND MACHINE INTELLIGENCE* (Issue 6).
- Peterson, C. H., & Black, R. (1988). Responses of growth to elevation fail to explain vertical zonation of suspension-feeding bivalves on a tidal flat. In *Oecologia* (Vol. 76).
- Phlips, E. J., Badylak, S., Lasi, M. A., Chamberlain, R., Green, W. C., Hall, L. M., Hart, J. A., Lockwood, J. C., Miller, J. D., Morris, L. J., & Steward, J. S. (2015). *From Red Tides to Green and Brown Tides: Bloom Dynamics in a Restricted Subtropical Lagoon Under Shifting Climatic Conditions* (Vol. 38, Issue 3).

- Pieterse, A., Puleo, J. A., Mckenna, T. E., & Aiken, R. A. (2015). Near-bed shear stress, turbulence production and dissipation in a shallow and narrow tidal channel. *Earth Surface Processes and Landforms*, 40(15), 2059–2070. <https://doi.org/10.1002/esp.3782>
- Price, W. A. (1954). Oyster reefs of the Gulf of Mexico. *Fishery Bull. Fish Wildlife Service U.S.*, 89–491.
- Reidenbach, M. A., Berg, P., Hume, A., Hansen, J. C. R., & Whitman, E. R. (2013). Hydrodynamics of intertidal oyster reefs: The influence of boundary layer flow processes on sediment and oxygen exchange. *Limnology and Oceanography: Fluids and Environments*, 3(1), 225–239. <https://doi.org/10.1215/21573689-2395266>
- Reidenbach, M. A., Koseff, J. R., & Monismith, S. G. (2007). Laboratory experiments of fine-scale mixing and mass transport within a coral canopy. *Physics of Fluids*, 19(7). <https://doi.org/10.1063/1.2752189>
- Reidenbach, M. A., Monismith, S. G., Koseff, J. R., Yahel, G., & Genin, A. (2006). Boundary layer turbulence and flow structure over a fringing coral reef. *Limnology and Oceanography*, 51(5), 1956–1968. <https://doi.org/10.4319/lo.2006.51.5.1956>
- Ridge, J. T., Rodriguez, A. B., Joel Fodrie, F., Lindquist, N. L., Brodeur, M. C., Coleman, S. E., Grabowski, J. H., & Theuerkauf, E. J. (2015). Maximizing oyster-reef growth supports green infrastructure with accelerating sea-level rise. *Scientific Reports*, 5. <https://doi.org/10.1038/srep14785>
- River, J., Joseph, V., & Dealteris, T. (1988). *The Geomorphic Development of Wreck Shoal, a Subtidal Oyster Reef of the* (Vol. 11, Issue 4).
- Rodriguez, A. B., Fodrie, F. J., Ridge, J. T., Lindquist, N. L., Theuerkauf, E. J., Coleman, S. E., Grabowski, J. H., Brodeur, M. C., Gittman, R. K., Keller, D. A., & Kenworthy, M. D. (2014). Oyster reefs can outpace sea-level rise. *Nature Climate Change*, 4(6), 493–497. <https://doi.org/10.1038/nclimate2216>

- Roegner, G. C., & Mann, R. (1995). *Early recruitment and growth of the American oyster Crassostrea virginica (Bivalvia: Ostreidae) with respect to tidal zonation and season.*
- Salvador de Paiva, J. N., Walles, B., Ysebaert, T., & Bouma, T. J. (2018). Understanding the conditionality of ecosystem services: The effect of tidal flat morphology and oyster reef characteristics on sediment stabilization by oyster reefs. *Ecological Engineering*, 112, 89–95.  
<https://doi.org/10.1016/j.ecoleng.2017.12.020>
- Schlichting H Gersten K. (2000). *Boundary layer theory* (8th ed.). Springer.
- Shumway, S. E. (1996). *Natural Environmental Factors.*  
<https://www.researchgate.net/publication/262728827>
- Smaal, A. C., Kater, B. J., & Wijsman, J. (2009). Introduction, establishment and expansion of the Pacific oyster *Crassostrea gigas* in the Oosterschelde (SW Netherlands). *Helgoland Marine Research*, 63(1), 75–83. <https://doi.org/10.1007/s10152-008-0138-3>
- Small, C., & Nicholls, R. J. (2003). A Global Analysis of Human Settlement in Coastal Zones. In *Source: Journal of Coastal Research* (Vol. 19, Issue 3). <https://about.jstor.org/terms>
- Smith, G. F., Roach, E. B., & Bruce, D. G. (2003). The location, composition, and origin of oyster bars in mesohaline Chesapeake Bay. *Estuarine, Coastal and Shelf Science*, 56(2), 391–409.  
[https://doi.org/10.1016/S0272-7714\(02\)00191-9](https://doi.org/10.1016/S0272-7714(02)00191-9)
- Smith, N. P. (1990). *Atmospheric and Océanographie Sciences AN INTRODUCTION TO THE TIDES OF FLORIDA'S INDIAN RIVER LAGOON II. CURRENTS.* <https://about.jstor.org/terms>
- Smith, N. P. (1993). *Tidal and Nontidal Flushing of Florida's Indian River Lagoon* (Vol. 16, Issue 4).

- Steward, J. S., Virnstein, R. W., Lasi, M. A., Morris, L. J., Miller, J. D., Hall, L. M., & Tweedale, W. A. (2006). The Impacts of the 2004 Hurricanes on Hydrology, Water Quality, and Seagrass in the Central Indian River Lagoon, Florida. *Estuaries and Coasts*, *29*, 954–965.
- Stiner, J. L., & Walters, L. J. (2008). EFFECTS OF RECREATIONAL BOATING ON OYSTER REEF ARCHITECTURE AND SPECIES INTERACTIONS. In *Source: Florida Scientist* (Vol. 71, Issue 1). Winter.  
<https://www.jstor.org/stable/24321467>
- Styles, R. (2015). Flow and Turbulence over an Oyster Reef. *Journal of Coastal Research*, *31*(4), 978–985.  
<https://doi.org/10.2112/JCOASTRES-D-14-00115.1>
- Sumer, B. M., Chua, L. H. C., Cheng, N.-S., & Fredsøe, J. (2003). Influence of Turbulence on Bed Load Sediment Transport. *Journal of Hydraulic Engineering*, *129*(8), 585–596.  
<https://doi.org/10.1061/ASCE0733-94292003129:8585>
- Temmerman, S., Meire, P., Bouma, T. J., Herman, P. M. J., Ysebaert, T., & De Vriend, H. J. (2013). Ecosystem-based coastal defence in the face of global change. In *Nature* (Vol. 504, Issue 7478, pp. 79–83). <https://doi.org/10.1038/nature12859>
- Wahl, T. L. (2003). Discussion of “Despiking Acoustic Doppler Velocimeter Data” by Derek G. Goring and Vladimir I. Nikora (Vol. 128, Issue 1).
- Wallace, J. M. (2016). Quadrant Analysis in Turbulence Research: History and Evolution. *Annual Review of Fluid Mechanics*, *48*, 131–158. <https://doi.org/10.1146/annurev-fluid-122414-034550>
- Wallace, J. M., Eckelmann, H., & Brodkey, R. S. (1972). The wall region in turbulent shear flow. In *J. Fluid Mech* (Vol. 54, Issue 1).

- Walters, L. J., Sacks, P. E., & Campbell, D. E. (2020). *Boating impacts and boat-wake resilient restoration of the eastern oyster Crassostrea virginica in Mosquito*.  
<https://www.researchgate.net/publication/353298818>
- Weaver, R. J., Johnson, J. E., & Ridler, M. (2016). Wind-Driven Circulation in a Shallow Microtidal Estuary: The Indian River Lagoon. *Journal of Coastal Research*, 32(6), 1333–1343.  
<https://doi.org/10.2112/JCOASTRES-D-15-00046.1>
- Whitman, E. R., & Reidenbach, M. A. (2012). Benthic flow environments affect recruitment of *Crassostrea virginica* larvae to an intertidal oyster reef. *Marine Ecology Progress Series*, 463, 177–191. <https://doi.org/10.3354/meps09882>
- Wiberg, P. L., Taube, S. R., Ferguson, E., Kremer, M. R., & Reidenbach, M. A. (2019). Wave Attenuation by Oyster Reefs in Shallow Coastal Bays. *Estuaries and Coasts*, 42(2), 331–347.  
<https://doi.org/10.1007/s12237-018-0463-y>
- Wiles, P. J., Rippeth, T. P., Simpson, J. H., & Hendricks, P. J. (2006). A novel technique for measuring the rate of turbulent dissipation in the marine environment. *Geophysical Research Letters*, 33(21).  
<https://doi.org/10.1029/2006GL027050>
- Woods, H., Hargis, W. J., Hershner, C. H., & Mason, P. (2005). Disappearance of the natural emergent 3-dimensional oyster reef system of the James River, Virginia, 1871-1948. *Journal of Shellfish Research*, 24(1), 139–142. [https://doi.org/10.2983/0730-8000\(2005\)24\[139:DOTNED\]2.0.CO;2](https://doi.org/10.2983/0730-8000(2005)24[139:DOTNED]2.0.CO;2)
- Wright, L. D., Gammisch, R. A., & Byrne, R. J. (1990). Hydraulic Roughness and Mobility of Three Oyster-Bed Artificial Substrate Materials. In *Source: Journal of Coastal Research* (Vol. 6, Issue 4).
- Yager EM, Venditti JG, Smith HJ, & Schmeeckle MW. (2018). The trouble with shear stress. *Geomorphology*, 41–50. <https://doi.org/https://doi.org/10.1016/j.geomorph.2018.09.008>.

Yang, J. Q., Chung, H., & Nepf, H. M. (2016). The onset of sediment transport in vegetated channels predicted by turbulent kinetic energy. *Geophysical Research Letters*, 43(21), 11,261-11,268.  
<https://doi.org/10.1002/2016GL071092>